Quaternary Science Reviews 103 (2014) 1–18

Contents lists available at ScienceDirect

Quaternary Science Reviews

journal homepage: www.elsevier.com/locate/quascirev

Invited review

# The Indian Ocean Zonal Mode over the past millennium in observed and modeled precipitation isotopes

Bronwen Konecky [a, *], James Russell [a], Mathias Vuille [b], Kira Rehfeld [c]

[a] Department of Geological Sciences, Brown University, Box 1846, Providence, RI, 02912, USA
[b] Department of Atmospheric and Environmental Sciences, University at Albany, SUNY, 1400 Washington Ave., Albany, NY, 12222, USA
[c] Alfred-Wegener-Institut Helmholtz-Zentrum für Polar- und Meeresforschung, Telegrafenberg A43, 14463, Potsdam, Germany

ARTICLE INFO

*Article history:*
Received 19 October 2013
Received in revised form
18 August 2014
Accepted 22 August 2014
Available online

*Keywords:*
Indian Ocean Zonal Mode
Indian Ocean Dipole
Last millennium
Precipitation isotopes

ABSTRACT

The Indian Ocean Zonal Mode (IOZM) has gained considerable attention in the past decade due to its role in causing widespread flooding and droughts in the continents and islands surrounding the Indian Ocean. The IOZM has also been observed to vary on a low-frequency (multi-decadal) basis, making its behavior important to understand both for mid-range 21st century climate prediction and for paleoclimate studies. Despite efforts to reconstruct the IOZM using corals and other high-resolution proxies, nonstationarities in the response of paleoclimate proxies to the IOZM have also been noted, raising the possibility that the IOZM may be difficult to reconstruct or to predict in the long-term. It is therefore critical to assess the low-frequency component of the IOZM in observed, modeled, and paleoclimate data from the Indian Ocean region in order to identify nonstationary behavior and to assess its role in low-frequency climate variations.

We present an analysis of low-frequency and nonstationary behavior in the IOZM on multi-decadal to centennial timescales using a combination of modeled, observed, and proxy reconstructions of $\delta^{18}O$/$\delta D_{precip}$. In order to assess multiple timescales of low-frequency variability, we focus on two key time periods: the historical period (1870–2003), and the past millennium (1000 C.E.-present). We find significant nonstationarities in the relationships between the IOZM, precipitation amount, and $\delta^{18}O_{precip}/\delta D_{precip}$ during the historical period. These relationships vary on a multi-decadal basis in our model and in observed/reanalysis datasets. Air-sea interactions in the Indo-Pacific Warm Pool and teleconnections to the Pacific Ocean, as well as the phase of the IOZM itself, may contribute to this nonstationary behavior.

We examine the potential ramifications of nonstationary IOZM behavior using a synthesis of spatially distributed proxy archives of $\delta^{18}O_{precip}/\delta D_{precip}$ from both sides of the IOZM region spanning the past millennium. Our findings indicate that during the past millennium, a strong IOZM-like connection exists in the proxy data network, with anti-correlation between East Africa and Indonesia. However, the links are spatially limited and in some cases timescale-dependent. Nonlinear behaviors in these links suggest that the IOZM may be difficult to detect on a consistent basis in proxy records from the past millennium. Based on our modeling results, the inconsistent links in the IOZM proxy network may arise from temporally and spatially variable relationships between the IOZM, precipitation, and $\delta^{18}O_{precip}/\delta D_{precip}$. We conclude that the IOZM's potential to influence the climate of the Indian Ocean region is inconsistently reflected in proxy data, and that due to the changing strength of the IOZM/$\delta^{18}O_{precip}/\delta D_{precip}$ relationship, its spatial "footprint" may be restricted on multi-decadal to multi-centennial timescales.



## 1. Introduction

### 1.1. The Indian Ocean Zonal Mode

The Indian Ocean Zonal Mode (IOZM; also known as the Indian Ocean Dipole; Table 1) is an important mode of interannual rainfall variability in the circum-Indian Ocean region (Saji et al., 1999). IOZM events occur during boreal Fall (September–December;

* Corresponding author. Tel.: +1 303 492 1143.
*E-mail address:* bronwen_konecky@alumni.brown.edu (B. Konecky).

http://dx.doi.org/10.1016/j.quascirev.2014.08.019
0277-3791/

**Table 1**
List of abbreviations.

| | |
|---|---|
| IOZM | Indian Ocean Zonal Mode |
| IOZM+(−) | IOZM positive (negative) |
| SST | Sea Surface Temperature |
| EEIO | Eastern Equatorial Indian Ocean |
| WEIO | Western Equatorial Indian Ocean |
| OND | October–December |
| SOND | September–December |
| ENSO | El Niño-Southern Oscillation |
| DMI | Dipole Mode Index |
| ZWI | Zonal Wind Index |
| LS | Link Strength |

SOND) every 2–7 years, causing pronounced rainfall anomalies in East Africa, western Indonesia, Australia, and India (e.g., Ashok et al., 2001; Black et al., 2003). Under normal conditions, a strong gradient in sea surface temperature (SST) between the warmer Eastern Equatorial Indian Ocean (EEIO) and the cooler Western Equatorial Indian Ocean (WEIO) causes weak westerly winds along the equator, contributing to the normal Indian Ocean Walker Circulation, with rising air and deep atmospheric convection over Indonesia and descending air and dry conditions in East Africa. During IOZM positive (IOZM+) events, a breakdown of the normal SST gradient and equatorial wind field leads to anomalously dry conditions in western Indonesia while enhancing the October–December (OND) rainy season in East Africa (Fig. 1). The event ceases when the normal boreal summer monsoon circulation develops, cooling the WEIO and relaxing anomalous easterly winds (Webster et al., 1999; Schott and McCreary, 2001).

In addition to its direct effects on East African and Indonesian precipitation, the IOZM has the ability to effect large changes in regional hydrology through its connection with the Indian monsoon and the El Niño-Southern Oscillation (ENSO) (Ashok et al., 2001; D'Arrigo and Smerdon, 2008; Ummenhofer et al., 2011). Both an IOZM+ event and an El Niño event necessitate anomalous cooling in the Indo-Pacific warm pool and weakened vertical ascent and convection over Indonesia, and in some but not all years the two co-occur (Saji et al., 1999; Saji and Yamagata, 2003a), possibly triggered by ENSO-induced zonal shifts in Walker cell anomalies (Fischer et al., 2005). IOZM+ events can also be triggered by meridional Hadley cell perturbations in the absence of ENSO dynamics (Fischer et al., 2005), and numerous other studies have established that the IOZM's interannual fluctuations are distinct from ENSO and should be considered a separate Indian Ocean phenomenon (e.g., Saji and Yamagata, 2003b; Behera et al., 2006; Schott et al., 2009).

While the IOZM operates independently from ENSO, teleconnections to the Pacific Ocean can play an important role in triggering and enhancing IOZM events via local air-sea interactions, ocean dynamics, and atmospheric teleconnections (Li et al., 2003; Behera et al., 2006; Gnanaseelan and Vaid, 2010). Interannual to decadal variability in Pacific SSTs can induce stronger/more frequent IOZM+ events by preconditioning the EEIO with a shallower thermocline (Annamalai et al., 2005; Schott et al., 2009). This preconditioning is associated with changes in the Indonesian Throughflow as well as an atmospheric teleconnection to equatorial winds over the Indian Ocean (Annamalai et al., 2005). Air-sea interactions in the warm pool are also integral to the generation and termination of IOZM events (Cai et al., 2013 and refs therein). SST variability in the EEIO induces a positive feedback with wind speed and evaporative heat loss, further enhancing cold anomalies. However, cool SSTs also suppress clouds and convection, warming the EEIO via increased shortwave radiation (Cai et al., 2013).

In addition to pronounced interannual variability, the IOZM also exhibits low-frequency variability. The power spectrum of observed IOZM SSTs exhibits a spectral peak at ~10 years (90% significance level), suggesting that periodicity at decadal and potentially longer timescales is intrinsic to the IOZM system (Ashok et al., 2004a, 2003). Twentieth century SST observations reveal multi-decadal modulations of the IOZM, with periods of time characterized by more frequent/intense IOZM negative (IOZM-) events (~1880–1920), more frequent/intense IOZM positive

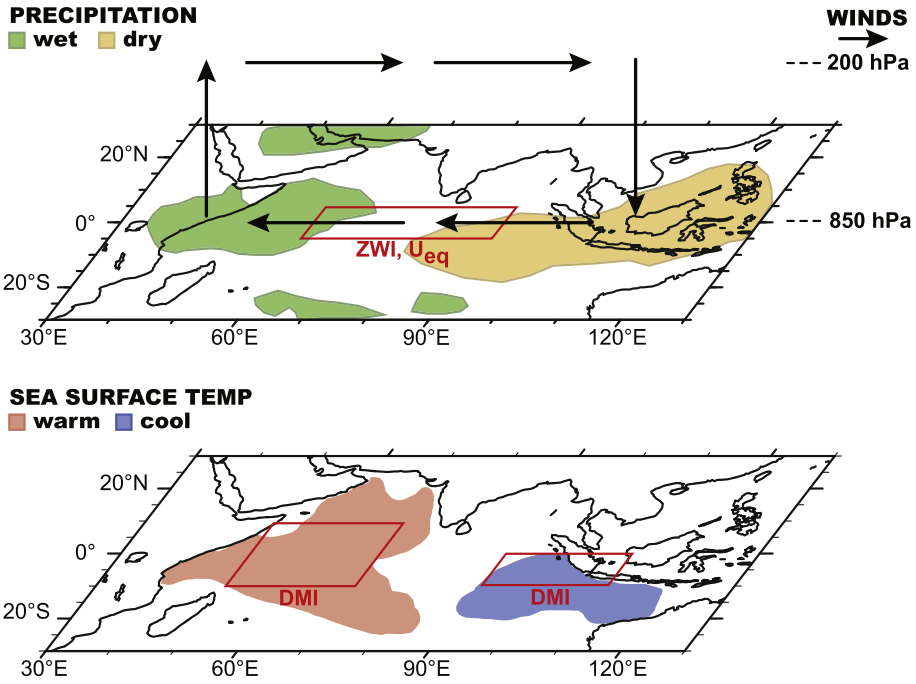


**Fig. 1.** Schematic illustration of the anomalous components of wind, precipitation, and sea surface temperature observed during an IOZM positive event. Adapted from Saji et al. (1999), Saji et al. (2006), and Schott et al. (2009). Red boxes outline the regions used to calculate the Zonal Wind Index, $U_{eq}$, and the Dipole Mode Index, discussed in text.

(IOZM+) events (~1960–2000), and periods of lower overall activity (~1920–1950) (Kripalani and Kumar, 2004; Ihara et al., 2008). Multi-decadal variations in the equatorial Indian Ocean windfield, SST, and thermocline depth are also apparent in observations and in modeling simulations (Saji and Yamagata, 2003b; Ashok et al., 2004a; Annamalai et al., 2005; Tozuka et al., 2007).

Low-frequency behavior makes the IOZM potentially important to and detectible in low-resolution paleoclimate proxy reconstructions. Indeed, paleoclimate studies have invoked "IOZM-like" dynamics to explain low-frequency patterns in regional paleoclimate from decadal up to orbital timescales (e.g., Stager et al., 2005; Griffiths et al., 2010; Gupta et al., 2010). These "IOZM-like" dynamics are not directly analogous to those of an individual IOZM event, whose onset and cessation are directly tied to a given year's seasonal cycle. However, a low-frequency, "IOZM-like" mode could arise from periods of more frequent/intense IOZM events (e.g., Tozuka et al., 2007), intrinsic low-frequency variability in Indian Ocean surface ocean characteristics (e.g., Annamalai et al., 2005), and/or feedbacks with the Indian monsoon circulation and the Indonesian Throughflow (Ashok et al., 2001; Annamalai et al., 2003, 2005).

Understanding low-frequency variations in the IOZM is critical for decadal-to century-scale climate prediction in the circum-Indian Ocean region. This is particularly true under 21$^{st}$ century global climate change scenarios, as a recent increase in IOZM intensity has been linked to increased greenhouse gas concentrations and warming (Cai et al., 2009) and increasingly strong positive feedbacks with the Asian monsoon circulation (Abram et al., 2008). However, future variability of the IOZM is uncertain due to uncertainties in ENSO and Asian monsoon teleconnections (Abram et al., 2008; Cai et al., 2009), which are strongly affected by inter-decadal variability in the Pacific Ocean (Zhang et al., 1997; Ashok et al., 2004a). In some model simulations, changes in the mean state of the tropical Indian and Pacific Oceans are associated with increased frequency of IOZM+ events, particularly events occurring in consecutive years (Saji et al., 2006; Cai et al., 2009). However, IOZM event frequency may not increase in the 21$^{st}$ century, despite a mean state of the Indian Ocean that is projected to become more "IOZM+ -like" in its mean wind and SST structure (Cai et al., 2013).

Paleoclimate records can help to illuminate the interactions between IOZM intensity, low-frequency variability, and changes in mean state. On paleoclimate timescales, corals, lake level records, tree rings, and output from paleoclimate model simulations have all been interpreted to reflect IOZM variability on interannual to multidecadal time-scales (e.g., Stager et al., 2005; Zhao et al., 2005; Abram et al., 2008, 2007; D'Arrigo et al., 2008). However, recent paleoclimate proxy reconstructions and model simulations suggest that continental rainfall in the circum-Indian Ocean region has a nonstationary relationship with Indian Ocean SST variability on decadal and longer timescales (Zinke et al., 2009; Coats et al., 2013). The relationship between Indian Ocean regional rainfall and ENSO, as well as IOZM teleconnections, may also be nonstationary on these timescales (Ashok et al., 2001, 2004b; Timm et al., 2005). Unstable behavior in the IOZM itself, and/or nonstationarity in the IOZM's relationship with rainfall, must be addressed in order to improve our understanding of the role of the IOZM in paleoclimate as well as its role in regulating regional precipitation variability in the future.

### 1.2. Tracking past and present IOZM variations with precipitation isotopes

Oxygen and hydrogen isotopes of precipitation ($\delta^{18}O_{precip}$ and $\delta D_{precip}$) are an increasingly important proxy for modern and past climate processes in the tropics (e.g., Vuille et al., 2012; Conroy et al., 2013; Moerman et al., 2013). In the Indo-Pacific, changes in the Walker circulation associated with the IOZM alter rainfall as well as the O and H isotopic composition of rainfall in East Africa and Indonesia. These anomalies, observed in precipitation and precipitation isotopic data from stations distributed throughout East Africa and Indonesia, were reproduced by an isotope-enabled GCM simulation from 1950 to 1994 (Vuille et al., 2005a). The IOZM produces isotopic anomalies by altering the Walker circulation over the Indian Ocean, changing the rainout and distillation processes that accompany anomalous vertical ascent (descent), upper-level divergence (convergence), and increased (decreased) convection over East Africa (Indonesia) during the SOND season. Because both sides of the Walker cell are affected in an opposite manner, a distinctive east/west spatial pattern characterizes the precipitation isotopic response to the IOZM, with significant changes of opposite direction occurring in East Africa and Indonesia. IOZM+ events are associated with negative ($^{18}$O-, D-depleted) anomalies in East Africa and positive ($^{18}$O-, D-enriched) anomalies in western Indonesia.

An increasing number of high-resolution proxy records of $\delta^{18}O_{precip}$ and $\delta D_{precip}$ spanning the past millennium (1000 C.E.-present) is becoming available from sediments, corals, and speleothems in the circum-Indian Ocean region. These records have suggested considerable variations in hydrology over the past millennium (Zinke et al., 2004; Newton et al., 2006; Fleitmann et al., 2007; Partin et al., 2007; Sinha et al., 2007; Abram et al., 2008; Griffiths et al., 2010; Tierney et al., 2010, 2011; Yan et al., 2011; Konecky et al., 2013, 2014). Many but not all of these records are characterized by pronounced multi-decadal variability (Zinke et al., 2004; Fleitmann et al., 2007; Konecky et al., 2013), and some show distinctive centennial-scale features or even millennium-long trends (Tierney et al., 2011; Yan et al., 2011; Konecky et al., 2013, 2014). Changes in the Indian or Pacific Ocean Walker circulation have been proposed to explain O- and H-isotopic variations on all timescales, as well as interactions with the Indian, East Asian, and Australasian monsoon circulation. The Northern Hemisphere Medieval Climate Anomaly (MCA; ~1000–1200 C.E.) and Little Ice Age (LIA; 1550–1800 C.E.) have received particular attention, with potential ramifications for solar forcing and Northern Hemisphere climate changes to affect regional atmospheric circulation. The timing of these multi-century events varies from site to site, and age model uncertainties often preclude a direct comparison of these variations to each other and to Northern Hemisphere temperature records (Masson-Delmotte et al., 2013). Nonetheless, records from both sides of the Indian Ocean suggest that the Indian Ocean Walker circulation may have responded strongly to external forcings on multi-decadal and longer timescales, leading to both precipitation and isotopic anomalies over the continents (Griffiths et al., 2010; Tierney et al., 2013). This highlights the importance of systematically testing IOZM relationships in isotopic proxy records, especially records that directly track $\delta^{18}O_{precip}/\delta D_{precip}$.

In this study, we examine low-frequency behavior of the IOZM/$\delta^{18}O_{precip}$ (and IOZM/$\delta D_{precip}$) relationship over two important time periods: the historical period (1870–2003), and the past millennium (~1000 C.E. to present). The historical period, for which a critical mass of SST observations is available, provides the longest and best-constrained timeframe to observe IOZM behavior, including several multi-decadal cycles. The past millennium provides an important test case to observe multi-decadal to centennial variability in IOZM behavior and to assess its regional impacts. These proxy records comprise the only network of $\delta^{18}O_{precip}/\delta D_{precip}$-based proxy reconstructions from the core IOZM-affected regions of East Africa and Indonesia that are of high enough resolution to assess low-frequency timescales of variability over the past millennium. Together, these two timeframes provide

important insights into low-frequency behavior of the IOZM in data and proxy records, setting the stage for future data/model comparisons with longer isotope-enabled paleoclimate simulations.

We describe our methods in Section 2. In Section 3, we examine multi-decadal variations in the IOZM/$\delta^{18}O_{precip}$ relationship during the historical period using an isotope-enabled Atmospheric General Circulation Model (AGCM) experiment forced with observed SSTs. This simulation from the Stable Water Isotope INtercomparison Group (SWING) enables us to test the stationarity of the precipitation and precipitation isotopic response to the IOZM on a multi-decadal timescale, and to investigate the potential local and remote climate relationships that may contribute to enhancing or diminishing the IOZM's signal through time. In Section 4, we assess the role of the IOZM in rainfall variations in the Indian Ocean region over the past millennium using a synthesis of ~1 ka continental proxy reconstructions from East Africa and western Indonesia. We interpret these results in light of the SWING simulation, focusing especially on potential non-stationarities in the proxy response to the IOZM. In Section 5, we discuss the implications of our model and proxy synthesis results for studies of the IOZM, and for studies of Indian Ocean region climate over the past millennium.

## 2. Methods

### 2.1. Model and observational data

SWING Experiment S1B (http://atoc.colorado.edu/~dcn/SWING/index.php) is an atmosphere-only GCM (AGCM) simulation forced with observed monthly SST from the HadISST v1.1 global dataset. Stable water isotope tracers are fully incorporated into the atmosphere, allowing isotopic fractionation to occur during water phase changes and to be advected through the atmospheric water cycle. The ECHAM4 model configuration used for SWING S1B is as described in Vuille et al. (2005a). Several AGCMs have performed SWING Experiment S1B. We chose to focus on the ECHAM4 model, as it has been previously validated in the IOZM region with good results compared to observations of precipitation and $\delta^{18}O_{precip}$ (Vuille et al., 2005a, 2005b). The approach of using atmosphere-only GCM forced with prescribed SSTs avoids some of the problems in simulating intra-tropical teleconnections that often arise in fully coupled GCM simulations (e.g., Tierney et al., 2013). Pacific Ocean SSTs are teleconnected to Indian Ocean SSTs via an "atmospheric bridge," wherein adjustments in the Walker Circulation and related changes in subsidence, cloud cover, radiation receipts and wind stress result in SST anomalies in the Indian Ocean basin 1–6 months later (Klein et al., 1999). In an atmosphere-only GCM simulation, the impact of these processes on SSTs has already been prescribed. All analyses were performed on the SOND season, which contains the strongest observed IOZM/$\delta^{18}O_{precip}$ relationship; this season captures the peak of rainfall anomalies associated with perturbed Walker Circulation in East Africa (OND, Nicholson, 1997) and SW Indonesia (SON, Aldrian and Susanto, 2003).

Two indices are commonly used to describe the IOZM (Fig. 1): the Dipole Mode Index (DMI; Saji et al., 1999), based on the zonal SST gradient in the tropical Indian Ocean; and the Zonal Wind Index (ZWI), also known as $U_{eq}$, which is based on the low-level zonal wind speed anomaly along the equator in the central tropical Indian Ocean (Hastenrath et al., 1993; Hastenrath, 2005). These two indices produce similar identification of IOZM events over the observational period (Saji et al., 1999). During an IOZM+ event, anomalous easterly wind (u-wind) wind leads the ZWI to be negative, whereas the SST-based DMI is positive. We base our analyses on the ZWI, defined here as the SOND zonal wind speed anomaly at 850 hPa averaged over 60°–90°E, 4°N–4°S. Vuille et al. (2005a) have shown that this index is closely tied to interannual perturbations of the Walker circulation over the Indian Ocean and hence highly correlated with convective activity and $\delta^{18}O_{precip}$ variations over both SE Asia and East Africa.

We analyze simulated precipitation amount (P) and $\delta^{18}O_{precip}$ averaged over two 8° × 16° boxes (4 × 8 model grid cells) in tropical East Africa (6°S–2°N, 34°E–50°E) and southwest (SW) Indonesia (10°S–2°S, 106°E–122°E). These areas were chosen both to represent regions of strong ZWI/P correlation for the overall experiment (1870–2003), and to be centered on 5 of the 6 locations of the proxy records analyzed in Section 4. We also present simulated P and $\delta^{18}O_{precip}$ for an additional box over East Africa, shifted north by two degrees (4°S–4°N, 34°E–50°E), to evaluate the sensitivity of our results in East Africa in light of the spatial heterogeneity in the IOZM's precipitation isotopic response in that region.

When possible, we compare our results to 20th century wind, P, and $\delta^{18}O_{precip}$ observations. For model validation purposes we analyze winds from the NCEP/NCAR Reanalysis V1 (Kalnay et al., 1996), precipitation data from the CPC Merged Analysis of Precipitation (CMAP; Xie and Arkin, 1997), and precipitation isotopic data from the International Atomic Energy Agency's Global Network of Isotopes in Precipitation (GNIP; IAEA/WMO, 2006). Additional analyses are performed with monthly mean precipitation rate and wind field data from the NOAA 20th Century Reanalysis V2 (Compo et al., 2011). CMAP, NCEP/NCAR Reanalysis, and 20th Century Reanalysis data are available from http://www.esrl.noaa.gov/psd/, and GNIP data are available from http://isohis.iaea.org.

All cross-correlations and significance estimates presented in this paper take into account potential autocorrelation of the individual time series, and significance estimates are adjusted when necessary (i.e. the lag-1 autocorrelation coefficient lead to a substantial reduction in the degrees of freedom; see Mitchell et al., 1966).

### 2.2. Synthesis of 1 ka proxy reconstructions of precipitation isotopes in the IOZM region

For our proxy data synthesis, we selected all available records that: 1) span at least the past millennium (minimum age of the oldest sample ≤1000 C.E.); 2) contain at least 30 measurements between 1000 and 2000 C.E.; and 3) fall within the region of significant ZWI/P correlation ($p < 0.05$) during the main IOZM season (SOND) in modern precipitation observations (Fig. 2). Records vary in their length, so we restricted our analysis to the common time period ($N$) of 850 C.E. – 2000 C.E.

We employ a set of linear and nonlinear similarity estimators designed specifically for small but complex networks of paleoclimate time series (Rehfeld et al., 2012, 2011; Rehfeld and Kurths, 2014). Complex network studies are being increasingly employed in climate science to extract dynamical information from gridded, observational datasets based on the strength of connections between the time series from sets of grid points (Donges et al., 2009; Malik et al., 2011). This approach was recently modified for application to smaller data networks composed of spatially heterogeneous, unevenly time-sampled paleoclimate data, and it was successfully used to demonstrate connections between the Indian and Asian monsoon systems during the past millennium from a network of multiproxy records (Rehfeld et al., 2012).

Treating groups of time series as a complex network allows several types of similarities to be tested simultaneously, rather than making *a priori* assumptions about the variance contained in each record or set of records. Datasets do not need to be resampled to a common timestep, thus avoiding loss of high-frequency/

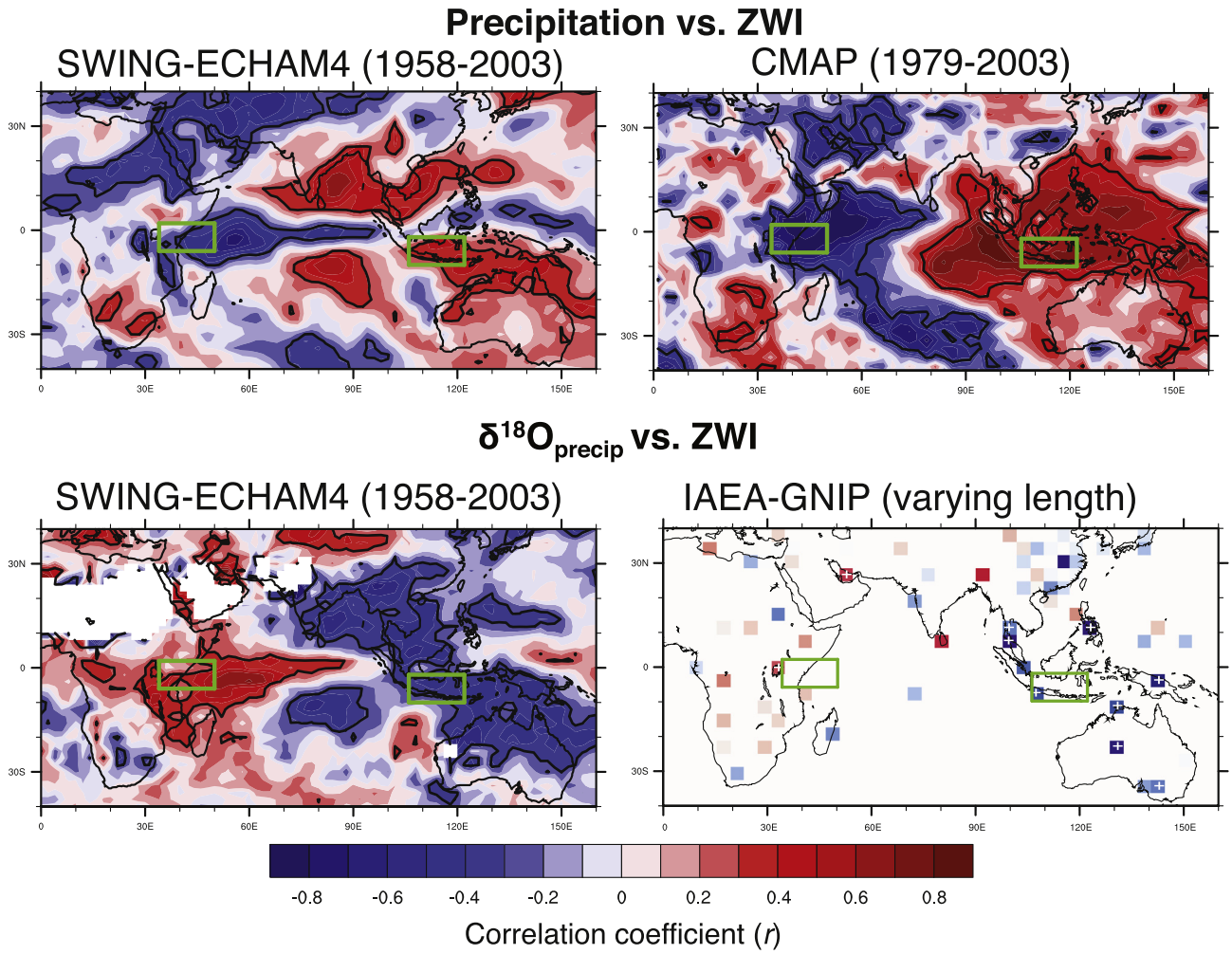


**Fig. 2.** Performance of ECHAM4 SWING S1B simulation (left) in simulating observed SOND precipitation (top) and isotopic (bottom) anomalies from 1958 to 2003. Shading represents the strength and sign of correlation, and black contours denote correlations where $p < 0.05$. In the lower-right figure, box shading denotes the strength and sign of correlation, and correlations significant at $p < 0.05$ are marked with a +. Green boxes denote the locations of East Africa and Southwestern Indonesia boxes used throughout our analysis of the SWING simulation. Precipitation data are from the CPC Merged Analysis of Precipitation (CMAP; available at http://www.esrl.noaa.gov/psd/data/gridded/data.cmap.html) from 1979 to 2003. Precipitation isotopic data are from the International Atomic Energy Agency-Global Network of Isotopes in Precipitation (GNIP; http://isohis.iaea.org).

overestimation of low-frequency variability and, resolution permitting, providing a means to assess even decadal-scale variance. This is achieved using Gaussian kernels, which more accurately estimate the cross-correlation functions between highly irregularly-sampled time series than linear interpolation or other kerneling techniques (Rehfeld et al., 2011). Both linear and nonlinear correlations are explored simultaneously by performing two pairwise similarity calculations, the nonlinear interrelation "mutual information" in addition to standard linear correlation. In total, we perform 4 similarity tests for each pair of time series within the network: linear cross-correlation (XCF) and nonlinear mutual information (MI), estimated using Gaussian kernels (gXCF, gMI) and the more traditional linear interpolation to an average timestep (iXCF, iMI) (Rehfeld and Kurths, 2014).

We first performed our analysis based on the published age models for each site in the network. We subtracted nonlinear trends from the records using a Gaussian kernel smoother with a width of $N/3$ (383.3 years), adapted for irregular sampling. This removes long-term trends in the data while preserving sub-decadal to multi-centennial variability (see Table 2 for a summary of timescales referred to in this study). Link strength (LS) (Rehfeld and Kurths, 2014) was computed for each pair of records in the network, with a possible range from 0 to 1, where a value of 0 means that no similarity estimators were significant at the 90% level, and a value of 1 means that all similarity estimators were significant at the 90% level. Since 4 similarity tests were used, LS can increase in increments of 0.25. The significance of these similarity estimates was determined using two-sided tests for zero correlation under the null hypothesis of the time series being sampled from autocorrelated red noise processes with the same lag-1 autocorrelation as the data. The critical values of the upper/lower confidence limits were estimated from 100 first-order autoregressive (AR(1)) processes, based on persistence estimated

**Table 2**
Definition of timescales.

| No. of years | Timescale of variability |
|---|---|
| 1–10 | Sub-decadal |
| 10–25 | Decadal |
| 25–100 | Multi-decadal |
| 100–300 | Centennial |
| 300–600 | Multi-centennial |
| 700–1150 | Long-term trend |

from least-squares regression and sampled at the same timesteps as the original records.

In order to test whether significant links found in our network analysis were robust when age model uncertainties were taken into account, we repeated our analysis using a simple iterative age modeling approach. We generated 100 new age models for each record using their radiometric age control points and their associated $1-\sigma$ errors. We selected a new age from within each age control point's range in a pseudorandom (random, but normally distributed) fashion, and then generated a new age model for each new set of age control points based on a fitting function that closely matched that used in the original, published age model. We then reassigned ages to each sample in the record, resulting in 100 new time series, and re-ran the similarity tests based on different pairs of age-perturbed time series. This method is similar in principle to other techniques for addressing age uncertainty in paleoclimate time series (Blaauw and Christen, 2011; Anchukaitis and Tierney, 2012). However, for this simple test, we operate on the assumption that errors on a given age/depth control point are normally distributed around the mean (i.e., published) age. We also assume that in developing the published age model functions, researchers have taken sedimentation rate changes, rejection of unlikely age control points, etc. into proper consideration, and therefore we opt to approximate published age/depth functions as best as possible rather than developing our own age/depth functions for each time series. We believe these are reasonable assumptions for a first-order test, although future studies could take into account other age error distributions, as well as other age/depth modeling functions.

For all age-uncertain ensembles, we calculated the ensemble mean link strength using combinations of detrending and smoothing of each time series, in order to isolate multi-decadal to multi-centennial variability among the sites, and to examine any timescale-dependent behavior in link strength. Low-frequency and high-frequency variability were removed via Gaussian kernel smoothing with a $\sigma$ of desired window width/2, with detrending windows of 100–1000 years in steps of 100 and smoothing windows of 1, 5, 10, and 25 years.

## 3. Precipitation and isotopic characteristics of the IOZM, 1870–2003

### 3.1. Simulation of observed IOZM-driven rainfall and $\delta^{18}O_{precip}$ variations with ECHAM4

Vuille et al. (2005a) demonstrated that ECHAM4 was able to reasonably simulate the SOND precipitation (P) and $\delta^{18}O_{precip}$ response to the IOZM in a shorter SWING experiment from 1950 to 1994. The longer SWING S1B experiment also provides a reasonable simulation of the seasonal cycle of precipitation and of interannual precipitation variability (not shown). The model simulates the P and $\delta^{18}O_{precip}$ response to the IOZM adequately, although it underestimates the spatial extent of the response in the P field, especially over continental East Africa, where the response is displaced eastward over the Indian Ocean (Fig. 2). The model more accurately simulates the spatial structure of the IOZM's influence on $\delta^{18}O_{precip}$. Broad regions of strong positive and negative ZWI/$\delta^{18}O_{precip}$ correlation are evident on the western and eastern poles of the IOZM, respectively, even in locations where the ZWI/P correlation is weaker (e.g., central Indonesia; Fig. 2). These differences in the IOZM's precipitation and precipitation isotopic footprint indicate that the IOZM's influence on $\delta^{18}O_{precip}$ is not restricted to changes in precipitation amount. Upstream fractionation and changes in vertical mixing, for example, could play a role in the IOZM/$\delta^{18}O_{precip}$ relationship at these locations.

In our focal areas in East Africa and SW Indonesia, P and $\delta^{18}O_{precip}$ are strongly negatively correlated throughout the simulation, with a Pearson correlation coefficient ($r$) of −0.81 and −0.88, respectively ($p < 0.05$; Table 3). A 25-year running correlation demonstrates that this relationship is stable on a multi-decadal basis, with $r$ ranging from −0.6 to −1 ($p < 0.05$; Fig. 3). This likely reflects a first-order control of precipitation amount on $\delta^{18}O_{precip}$ in these locations, as has been noted in observational studies from tropical regions (Dansgaard, 1964), although other factors such as moisture source and transport processes may weaken this relationship at times. Generally, the East African P/$\delta^{18}O_{precip}$ relationship is more variable (e.g., weakening between ~1900 and 1940), likely because East Africa receives precipitation from multiple oceanic and continental sources (Nicholson, 1996) which may differ isotopically (Levin et al., 2009; Costa et al., 2014). Even when $r$ weakens, however, the P/$\delta^{18}O_{precip}$ relationship remains significant at the 95% level.

### 3.2. Multi-decadal variations in the IOZM's influence on East African and SW Indonesian P, $\delta^{18}O_{precip}$

Vuille et al. (2005a) found strong correlations between the ZWI and $\delta^{18}O_{precip}$ in East Africa and SW Indonesia between 1950 and 1994 in a previous ECHAM simulation. Although ZWI/P and ZWI/$\delta^{18}O_{precip}$ are moderately correlated in East Africa and SW Indonesia when the entire 134-year S1B simulation is considered (Table 3), these relationships vary considerably on a multi-decadal basis. 25-year running correlations between ZWI/P and ZWI/$\delta^{18}O_{precip}$ in the two locations reveal that the $r$-value varies between 0 and |0.80| (Fig. 4). In East Africa, the correlations remain significant at the 95% level throughout the simulation ($|r| \geq 0.4$, $p < 0.05$). In SW Indonesia, however, the ZWI/$\delta^{18}O_{precip}$ and ZWI/P correlations are strong ($|r| \geq 0.4$, $p < 0.05$) from ~1945 to 1980 (with a brief exception around ~1965), but weak from ~1895 to 1930 ($|r| \leq 0.4$, $p > 0.05$).

These correlations do not necessarily reflect changes in the strength of the IOZM itself, but rather the response of precipitation amount and $\delta^{18}O_{precip}$ to IOZM variations. Two ~35-year periods, 1895–1930 and 1945–1980, correspond to decades when the IOZM's regional influence on P and $\delta^{18}O_{precip}$ in Indonesia was weaker and stronger, respectively. During these two periods, the simulated strength and spatial extent of the IOZM's influence on regional P and $\delta^{18}O_{precip}$ differs considerably from the 1870–2003 average, particularly over Indonesia (Fig. 5). From 1945 to 1980, the ZWI is correlated with P and $\delta^{18}O_{precip}$ across southern Indonesia, southeast Asia, the East African tropics and southern subtropics, and parts of the central and western Indian Ocean. From 1895 to 1930, however, the eastern edge of the IOZM influence disappears over Indonesia, while remaining in the central Indian Ocean. Perturbations to the low-level (850 hPa) wind field associated with the IOZM are notably absent over SW Indonesia during this time (Fig. S1), suggesting that IOZM events did not dramatically affect the low-level atmospheric circulation, and hence rainfall and $\delta^{18}O_{precip}$ in SW Indonesia. As P and $\delta^{18}O_{precip}$ remain highly correlated during this period (Fig. 3), climatic processes other than

**Table 3**
Correlation coefficients ($r$) between high-pass filtered SOND ZWI, P, and $\delta^{18}O_{precip}$.

| | East Africa | SW Indonesia |
|---|---|---|
| P/$\delta^{18}O$ | −0.81* | −0.88* |
| ZWI/P | −0.70* | 0.36* |
| ZWI/$\delta^{18}O$ | 0.59* | −0.33* |

*Denotes $p < 0.05$.

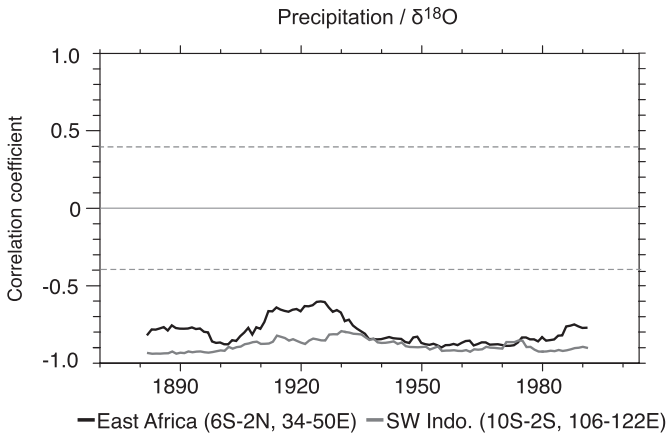


**Fig. 3.** 25-year running correlations between the precipitation amount and $\delta^{18}O_{precip}$ in the SWING simulation for East Africa (grey) and SW Indonesia (black). Dashed line represents the 95% significance level. Boxes are as in.Fig. 2.

the IOZM must have affected SW Indonesian P, and therefore $\delta^{18}O_{precip}$, more strongly than the IOZM.

Multi-decadal changes in the strength of the IOZM/P relationship are also evident in the 20th Century (20C) Reanalysis dataset (Fig. 6). The period of weakest correlation in the 20C reanalysis occurs between ~1920 and 1950, overlapping with but slightly later than the ECHAM4 simulation's weak ZWI/P correlation in SW Indonesia from 1895 to 1930. During these periods of weakened ZWI/P correlation, both the ECHAM4 simulation and the 20C reanalysis reveal a shift of the IOZM's spatial footprint away from the continents, particularly over Indonesia (Fig. S2). This indicates that IOZM's non-stationary influence on continental rainfall is a robust feature of the IOZM system, rather than an artifact of the SWING simulation or of ECHAM4. Differences in the timing of these weakened ZWI/P correlations likely arise from differences in the methods that ECHAM4 and 20C reanalysis models use to derive equatorial wind fields from SST (ECHAM4) or sea level pressure (20C reanalysis) observations. Additionally, ECHAM4 appears to underestimate the contraction of the IOZM's spatial footprint over continental East Africa, especially in the southeastern tropics (Fig. S2); this likely results in overestimates of the ZWI/P and ZWI/$\delta^{18}O_{precip}$ correlations in our East Africa box (Fig. 4). Indeed, when the East Africa box is shifted north by two degrees, ECHAM4 simulates a weaker ZWI/P correlation between 1920 and 1950, similar to the 20C reanalysis; the ZWI/$\delta^{18}O_{precip}$ correlation weakens below the 95% significance level around ~1915 and ~1945 (Fig. S3). Sites along the perimeter of the IOZM's spatial footprint, therefore, may be more sensitive to nonstationarities in the ZWI/P correlation through time.

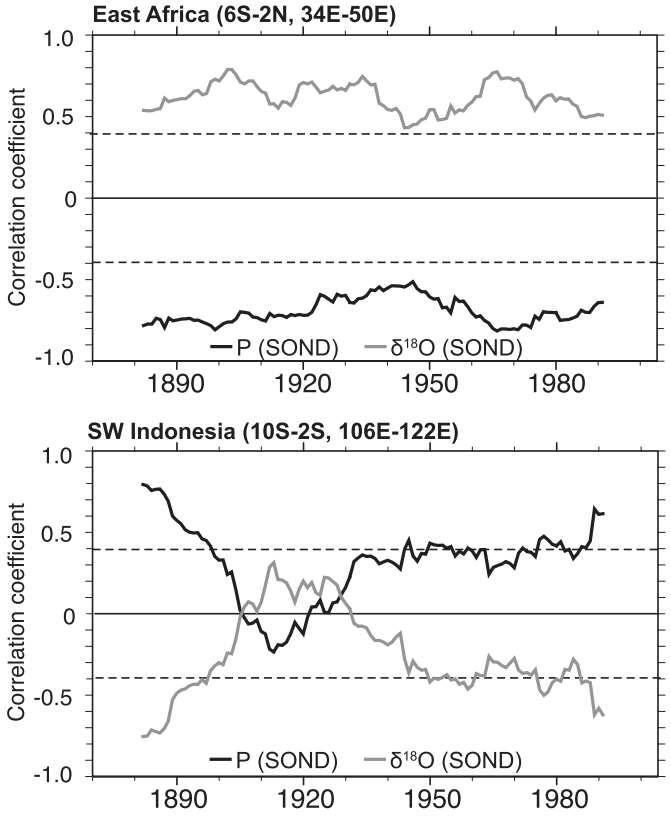


**Fig. 4.** Top: 25-year running correlations between SOND ZWI, precipitation, and $\delta^{18}O_{precip}$ during the SWING simulation for East Africa (top) and SW Indonesia (bottom). Refer to Fig. 2 for locations of East Africa and SW Indonesia boxes. Dashed lines denote the 95% significance level.

The phase of the IOZM may be partly responsible for modifying these atmospheric teleconnections. The IOZM was characterized by frequent and strong negative events between 1895 and 1930, and was in a more neutral phase between 1920 and 1950, with few strong positive or negative events (Ihara et al., 2008). The only period of time when ZWI and P are strongly correlated in both the SWING experiment and 20C reanalysis data is after 1950, when the IOZM entered a phase of frequent and strong positive events (Figs. 4 and 6). In the 20C reanalysis, IOZM+ events are more strongly correlated to East African and SW Indonesian P than IOZM-events, both generally (ZWI<0 and ZWI>0) and in the case of extreme events (ZWI < −1 and ZWI>1) (Table 4). Similarly, in the ECHAM4 SWING simulation, extreme IOZM+ events are more strongly correlated with SW Indonesian P than extreme IOZM− events. In East Africa, however, the IOZM− phase is more strongly correlated with P. In both regions, when all ZWI values are considered rather than extreme events only, the phase of the IOZM does not strongly influence the ZWI/P correlation. Although these results for East Africa are inconclusive, both the 20C reanalysis and ECHAM4 agree that the IOZM+ phase is more strongly represented in SW Indonesia than the IOZM− phase.

Both the SWING and the 20C reanalysis therefore suggest that precipitation in SW Indonesia, and possibly also East Africa, may more strongly reflect the IOZM when it is in a positive mode rather than in a negative mode or neutral mode. Because the IOZM-mode is essentially an anomalously strong pattern of “normal” SST and wind configurations in the Indian Ocean, it is possible that frequent/intense negative IOZM events do not modify the low-level atmospheric circulation over SW Indonesia to the same degree as positive IOZM events, leading to weaker ZWI/P correlation and hence weaker ZWI/$\delta^{18}O_{precip}$ correlation when negative events dominate. This finding has consequences for proxy records, indicating that IOZM+ behavior may be more easily detectible, especially in SW Indonesia.

Multi-decadal shifts in the IOZM's spatial and temporal imprint on P and $\delta^{18}O_{precip}$ have important ramifications for paleoclimate reconstruction of the IOZM, especially on multi-decadal timescales, and for its impacts on future precipitation. Proxy records from both sides of the Indian Ocean may move in and out of the IOZM's main zone of influence through time. This effect is most noticeable in SW Indonesia, where the IOZM's influence nearly disappears during periods of weak ZWI/$\delta^{18}O_{precip}$ correlation (Fig. 5). In tropical East Africa this effect is less obvious, but is more apparent at sites located at the periphery of the zone of strong ZWI/$\delta^{18}O_{precip}$ correlation, for example just two degrees northward of our main East

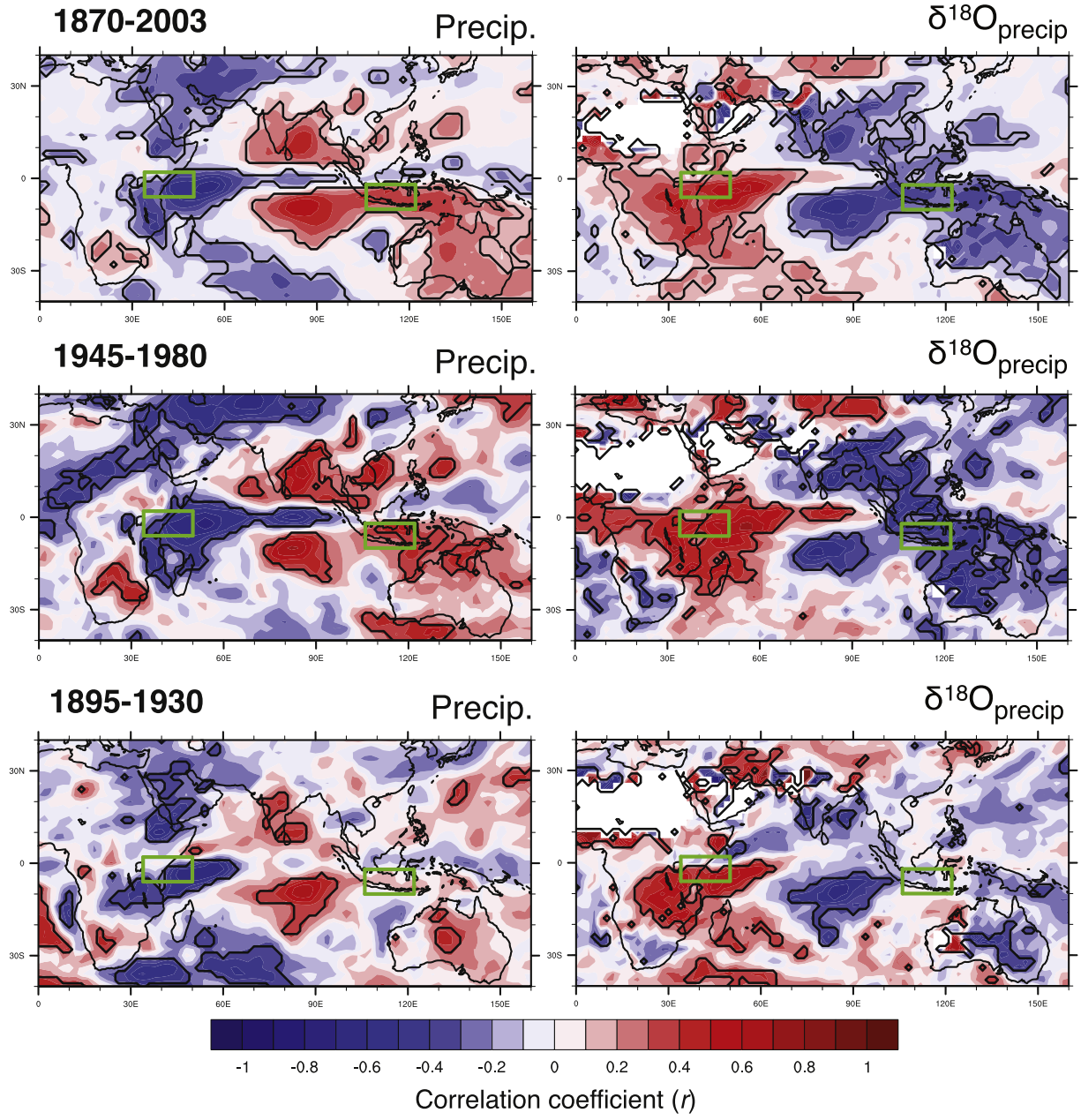


**Fig. 5.** Correlations between ZWI, P, and $\delta^{18}O_{precip}$ in the ECHAM4 SWING simulation. Top, full simulation (1870–2003). Middle, period of strong ZWI/$\delta^{18}O_{precip}$ correlation (1945–1980). Bottom, period of weak ZWI/$\delta^{18}O_{precip}$ correlation (1895–1930). Shading, black contours, and green boxes are as in.Fig. 2.

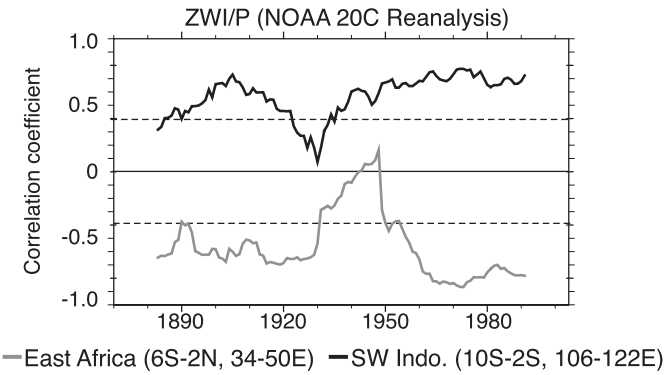


**Fig. 6.** As in Fig. 4, but for ZWI and precipitation in the NOAA Twentieth Century Reanalysis dataset. Grey line denotes East Africa and black line denotes SW Indonesia.

**Table 4**
Correlation coefficients between positive and negative ZWI and P in East Africa and Indonesia.

| | All | | Extremes | |
|---|---|---|---|---|
| | IOZM+ (ZWI < 0) | IOZM− (ZWI > 0) | IOZM+ (ZWI < −1) | IOZM− (ZWI > 1) |
| **NOAA 20C Reanalysis** | | | | |
| East Africa | −0.60 | −0.44 | −0.51 | −0.15 |
| SW Indonesia | 0.43 | 0.30 | 0.35 | 0.13 |
| **ECHAM4 SWING** | | | | |
| East Africa | −0.38 | −0.36 | −0.43 | −0.55 |
| SW Indonesia | 0.22 | 0.22 | 0.45 | 0.11 |

All values are significant at the 90% level when compared with 2000 uncorrelated surrogates (see text).

Africa box (Fig. S3). The SWING simulation may even underestimate the changing spatial footprint of the IOZM on continental East Africa, as the contracting zone of IOZM influence is more dramatic in 20C reanalysis data during a time period of poor ZWI/P correlation (Fig. S2).

In parts of East Africa, ZWI/P and ZWI/$\delta^{18}O_{precip}$ relationships are strong even when the P/$\delta^{18}O_{precip}$ relationship weakens. This reaffirms that the ZWI influences $\delta^{18}O_{precip}$ via multiple mechanisms, not just precipitation amount. Processes including upstream fractionation and intensified convection during IOZM events could explain why the IOZM's spatial footprint is broader across tropical Africa in $\delta^{18}O_{precip}$ than in P alone (Fig. 5, top). Therefore, while the IOZM's influence may wax and wane on individual proxy records of East African precipitation amount (Fig. S3), a network of $^{18}O$- and D-based proxy records could be promising in reconstructing IOZM behavior on multi-decadal timescales.

### 3.3. The role of tropical Pacific SST in modulating the IOZM's influence in SW Indonesia

#### 3.3.1. Interaction with the El Niño-Southern Oscillation

Interactions with ENSO could potentially modulate the IOZM's influence in SW Indonesia, as ENSO is both a key driver of interannual Indonesian rainfall variability (Aldrian and Susanto, 2003; Hendon, 2003) and may modulate IOZM strength on decadal timescales (Annamalai et al., 2005). ENSO events alter Indonesian rainfall by modifying the Pacific Walker cell, with warm events suppressing rainfall during the boreal summer dry season (JJA) and the onset of the monsoon (SON) (Hendon, 2003). On decadal and longer timescales, many studies have noted low-frequency "ENSO-like" SST modes in the Pacific Ocean (e.g., Zhang et al., 1997; Enfield and Mestas-Nuñez, 1999; Mantua and Hare, 2002; Krishnan and Sugi, 2003). Periods of enhanced/suppressed interannual ENSO activity, as well as "ENSO-like" behavior arising from low-frequency variations in Pacific SSTs, have been invoked to explain paleoclimatic phenomena throughout the Indo-Pacific, including Indonesia (Moy et al., 2002; Cobb et al., 2003; Conroy et al., 2008; Felis et al., 2012; Rodysill et al., 2012, 2013). ENSO also indirectly affects East African SOND rainfall via oceanic and atmospheric teleconnections to SST anomalies that occur during the ENSO development phase in boreal spring (Nicholson, 1997; Nicholson and Kim, 1997). Despite these teleconnections, East African P and $\delta^{18}O_{precip}$ remain strongly correlated to ZWI throughout the SWING simulation (Fig. 4); therefore, we focus our discussion on ENSO's effects on SW Indonesian P and $\delta^{18}O_{precip}$.

As is the case with ZWI, the correlation between the NINO3.4 index and SW Indonesian P and $\delta^{18}O_{precip}$ fluctuates throughout the SWING simulation (Fig. 7). Fig. 7 depicts the correlation between SW Indonesian P and $\delta^{18}O_{precip}$ with NINO3.4, the ENSO region with the greatest impact on convective anomalies in Indonesia (Hendon, 2003). Two 10–15 year periods of weakened NINO3.4/P and NINO3.4/$\delta^{18}O_{precip}$ correlation occur around ~1915 and ~1955. In the earlier event, the correlation between NINO3.4 and $\delta^{18}O_{precip}$ begins to weaken earlier (~1900) than its correlation with P, similar to the weakening of the ZWI/$\delta^{18}O_{precip}$ correlation.

When SW Indonesian P and $\delta^{18}O_{precip}$ experience the weakest relationship with the IOZM (~1895–1930), they also experience a weak relationship with ENSO (Fig. 7). However, the NINO3.4/P and NINO3.4/$\delta^{18}O_{precip}$ correlation is also weak in the 1950's, when the ZWI/P and ZWI/$\delta^{18}O_{precip}$ correlations are strong. Therefore, ENSO does not appear to be primarily responsible for modulating the ZWI/P and ZWI/$\delta^{18}O_{precip}$ correlation, as at times these correlations weaken together. The processes that weaken the IOZM's influence on P and $\delta^{18}O_{precip}$ in SW Indonesia thus could also affect ENSO's influence during these times.

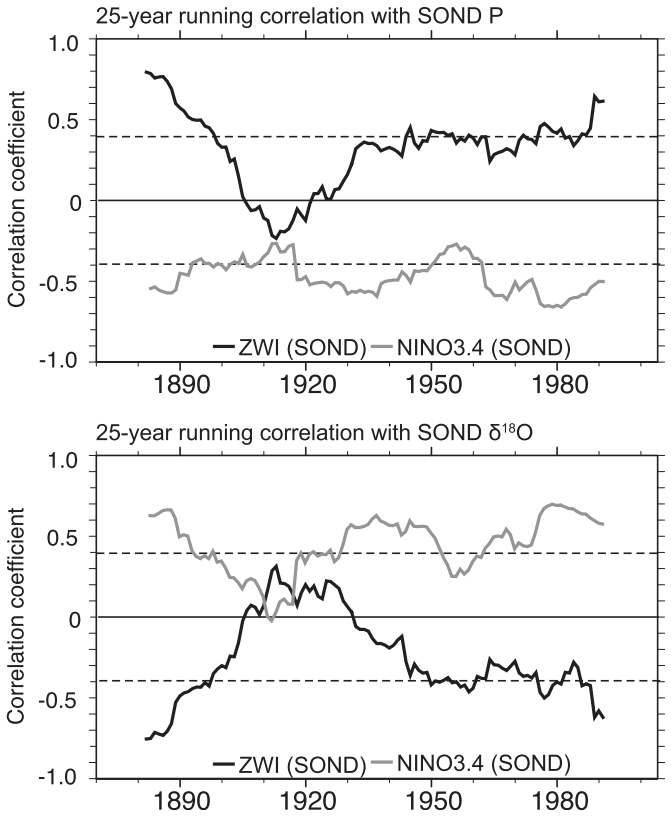


**Fig. 7.** Top: 25-year running correlations between SW Indonesian P (SOND), ZWI (SOND), and NINO3.4 (SOND) during the SWING simulation. Bottom: As in top, but for SW Indonesian $\delta^{18}O_{precip}$. Dashed lines denote the 95% significance level.

#### 3.3.2. Interaction with local sea surface temperature

To better understand potentially competing influences on the IOZM/P and IOZM/$\delta^{18}O_{precip}$ relationships in SW Indonesia, we examined the field correlations between P, $\delta^{18}O_{precip}$, and tropical SST during the two 50-year time periods that encompass the weakest and strongest ZWI/P and ZWI/$\delta^{18}O_{precip}$ correlations, 1880–1930 and 1930–1980, respectively. SST anomalies were calculated from the same HadISST dataset that was used to force the SWING simulation. Uncertainties in the HadISST dataset are larger further back in time due to sparser SST observations, especially in the southern oceans, yet examining the modeled atmospheric response to these SST observations can nonetheless provide a context for behavior of the ZWI at different time periods in the model under prescribed SST variations.

ECHAM4 simulates the canonical SST/ZWI correlations (Saji et al., 1999) reasonably well, with negative SST/ZWI correlation off the East African coast and positive SST/ZWI correlation southeast of Sumatra (Fig. S4). The ZWI/SST correlation in the eastern Indian Ocean is relatively constricted during SOND, whereas it is much stronger for SSTs during the boreal summer (not shown), as the effects of warm pool SST anomalies propagate westward in the Indian Ocean via downwelling Rossby waves (Webster et al., 1999; Gnanaseelan and Vaid, 2010).

Overall, the period of weakened ZWI/P and ZWI/$\delta^{18}O_{precip}$ correlation corresponds to a period of weaker influence of the Pacific during the boreal summer/IOZM development phase (MJJA), and stronger interactions with SSTs in the greater warm pool/western Pacific region. SOND P and $\delta^{18}O_{precip}$ in SW Indonesia are strongly correlated to SOND SSTs across much of the tropical Pacific during both 1880–1930 and 1930–1980 (Fig. 8). A tropical/subtropical correlation pattern extending to ~30° latitude in both hemispheres

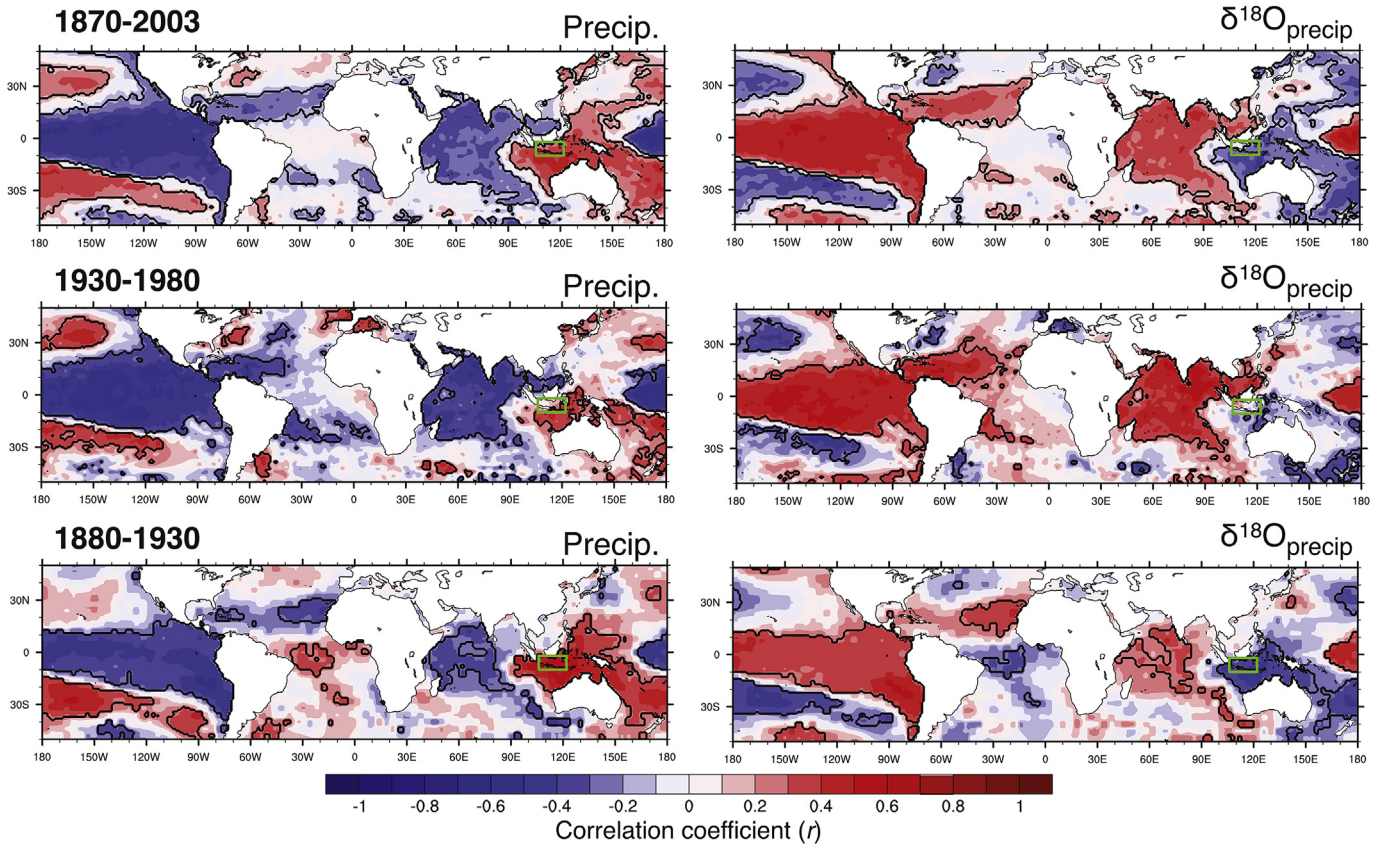


**Fig. 8.** Correlation between SW Indonesian P and $\delta^{18}O_{precip}$ (SOND) and SST (SOND). Top: the full SWING simulation (1870–2003). Middle: the period of strong ZWI/$\delta^{18}O_{precip}$ correlation in SW Indonesia (1945–1980). Bottom: the period of weak ZWI/$\delta^{18}O_{precip}$ correlation in SW Indonesia (1895–1930). Shading, black contours, and green box are as in Fig. 2. All data have been high-pass filtered to preserve interannual and subdecadal variability.

resembles patterns of low-frequency modes of SST variability in the Pacific, such as the Pacific Decadal Oscillation (PDO) or Pacific Multidecadal Variability (Zhang et al., 1997; Enfield and Mestas-Nuñez, 1999; Mantua and Hare, 2002; Krishnan and Sugi, 2003) (Fig. 8). This PDO-like correlation pattern with SOND SSTs is present in both time periods, suggesting that it does not interfere with the ZWI/P and ZWI/$\delta^{18}O_{precip}$ relationships in SW Indonesia. However, boreal summer (MJJA) SSTs also influence SW Indonesian rainfall (Hendon, 2003). The difference in the field correlations between the two time periods, 1880–1930 and 1930–1980, is highly apparent during MJJA (Fig. 9). From 1880 to 1930, when the ZWI/P and ZWI/$\delta^{18}O_{precip}$ correlations are weak in SW Indonesia (Fig. 4), SOND P and $\delta^{18}O_{precip}$ are strongly correlated with local SST (Fig. 9), as in SOND. The influence of remote SSTs in the tropical Pacific and the central Indian Ocean is much weaker during this time period compared with 1930–1980, when the ZWI correlation is strong.

During SOND, the biggest differences between 1880–1930 and 1930–1980 occur near SW Indonesia, the Indo-Pacific Warm Pool (IPWP), and northeast of Australia (Fig. 8). When the ZWI/P correlation is weaker (1880–1930), SW Indonesia P and $\delta^{18}O_{precip}$ are more strongly correlated to SSTs in southern Indonesia, throughout the IPWP, and in the W. Pacific. When the ZWI/P correlation is stronger, however (1930–1980), those influences are more limited compared with the influence of the tropical Pacific (Fig. 8). Therefore, it is possible that local and W. Pacific SST interactions during the SOND season may interfere with the ZWI/P and ZWI/$\delta^{18}O_{precip}$ relationships in SW Indonesia.

These findings indicate that Pacific sea surface dynamics may enhance the IOZM's influence on SW Indonesia rainfall, while local air-sea interactions may inhibit it. Previous modeling and observational studies have demonstrated the importance of teleconnections to the Pacific Ocean and local air-sea feedbacks in generating and amplifying IOZM events (Li et al., 2003; Behera et al., 2006; Gnanaseelan and Vaid, 2010; Cai et al., 2013). These teleconnections also influence the correlation between IOZM/ENSO, which has varied strongly during the past 50 years (Annamalai et al., 2005; Schott et al., 2009). Based on our results, it is possible that Pacific teleconnections and air-sea feedbacks may alter not just the strength and frequency of IOZM events and the strength of the IOZM/ENSO correlation, but also the strength of the correlations between ZWI/P and ZWI/$\delta^{18}O_{precip}$ in southwestern Indonesia.

### 3.3.3. *Effects of low-frequency SST variability on ZWI/P/$\delta^{18}O_{precip}$ relationships*

So far, our analyses have addressed non-stationarity of the interannual ZWI/$\delta^{18}O_{precip}$ relationship and ZWI/P relationships in the SWING simulation, as well as for 25-year moving windows within the SWING simulation. Periods of strong and weak correlation with the IOZM therefore reflect periods with enhanced/diminished frequency and/or magnitude of interannual IOZM events. Low-frequency variability in paleoclimate records is often attributed to time periods when interannual events tended towards one extreme or another. Indeed, observational and model evidence suggest that this is likely the nature of low-frequency IOZM variations (Tozuka et al., 2007). In their model, Pacific Ocean SST variability was important both for decadal, basin-wide warming/cooling of the Indian Ocean and for decadal modulation of interannual IOZM events (Tozuka et al., 2007).

It is also possible that a true low-frequency mode of variability exists in SST that could influence P/$\delta^{18}O_{precip}$ in East Africa and SW

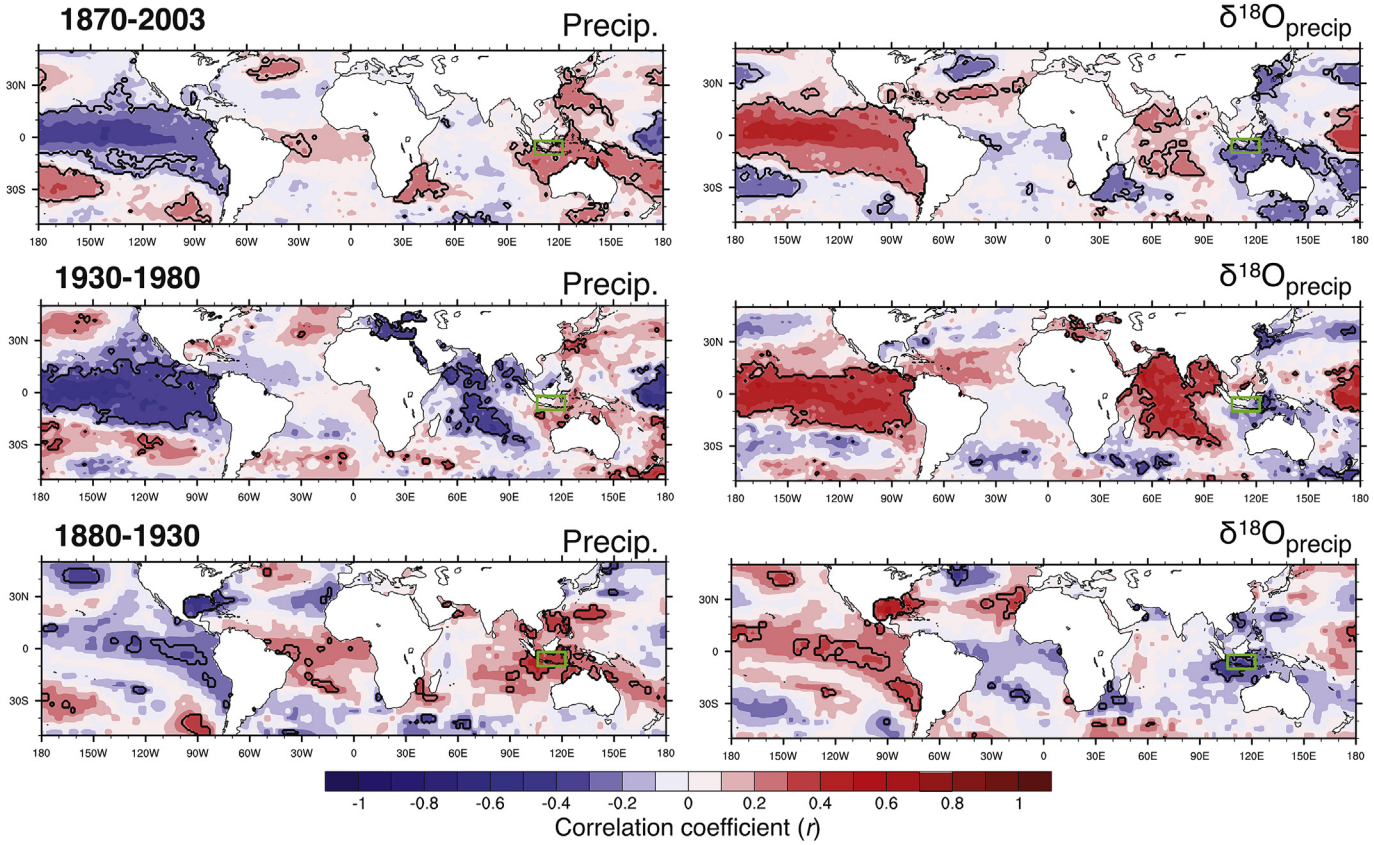


**Fig. 9.** As in Fig. 8, but between SW Indonesian P and $\delta^{18}O_{precip}$ (SOND) and SST (MJJA).

Indonesia. Previous work has suggested such SST variability to be influential on East African annual precipitation on timescales greater than 10 years in unforced model simulations of global climate (Tierney et al., 2013). The short duration of the SWING simulation prohibits a robust assessment of multi-decadal oscillations, but it is still possible to assess lower-frequency modes of variability by filtering interannual to subdecadal variations. We used a Lanczos low-pass filter with a cut-off frequency equivalent to 10 years to filter the SWING data. Correlation coefficients are presented in Table 5.

Overall, in SW Indonesia, interannual P and $\delta^{18}O_{precip}$ are moderately but significantly ($p < 0.05$) correlated to interannual variations in the ZWI (Table 3). SW Indonesian P, $\delta^{18}O_{precip}$, and ZWI correlations remain similar when high-frequency variations in P, $\delta^{18}O_{precip}$, and ZWI are removed (Table 5). In East Africa, the correlations between ZWI and P and $\delta^{18}O_{precip}$ are strong on an interannual basis (Table 3), but weaken substantially when high-frequency variations are removed (Table 5). The decadal East African ZWI/$\delta^{18}O_{precip}$ correlation is significant at the 95% level, but the decadal ZWI/P relationship is not ($p = 0.11$). Note that low-pass filtering introduces some degree of autocorrelation into the time series. The significance of these correlations decreases substantially when autocorrelation is taken into account, with none of the r-values in Table 5 remaining significant at the 95% level. Qualitatively, however, the influence of the IOZM on East African rainfall appears to be largely an interannual phenomenon in the SWING simulation, whereas its influence on SW Indonesian rainfall is apparent at both interannual and decadal frequencies.

**Table 5**
Correlation coefficients ($r$) between low-pass filtered SOND ZWI, P, and $\delta^{18}O_{precip}$.

| | East Africa | SW Indonesia |
|---|---|---|
| P/d18O | −0.80* | −0.88* |
| ZWI/P | −0.14 | 0.30* |
| ZWI/d18O | 0.17* | −0.30* |

*Denotes $p < 0.05$. Note that no $r$-values in the table remain significant at the 95% level if autocorrelation (lag-1) of low-pass filtered time series has been taken into account.

Low-frequency SST variability in the Pacific Ocean may play a role in the weaker ZWI/P and ZWI/$\delta^{18}O_{precip}$ relationships in SW Indonesia. In East Africa, correlations between tropical Pacific SST and P and $\delta^{18}O_{precip}$ are much stronger on a decadal basis than an interannual basis (Fig. 10). In SW Indonesia, on the other hand, correlations between P, $\delta^{18}O_{precip}$, and tropical Pacific SSTs are similar on both timescales. In other words, SW Indonesia is strongly influenced by tropical Pacific SSTs on an interannual as well as a decadal basis, which could help explain the only moderate correlations between ZWI/P and ZWI/$\delta^{18}O_{precip}$ (Tables 3 and 4). It is possible that these interactions between SST, P, and $\delta^{18}O_{precip}$ make the ZWI more vulnerable to nonstationary correlations with P and $\delta^{18}O_{precip}$ in SW Indonesia (Fig. 4). In East Africa, Pacific SSTs are not highly influential unless interannual variability is removed (Fig. 10), which could help to explain the stronger interannual ZWI/P and ZWI/$\delta^{18}O_{precip}$ correlations there (Table 3), as well as the ZWI's more stationary relationship with P and $\delta^{18}O_{precip}$ (Fig. 4). Indeed, when interannual and sub-decadal variability are filtered out, the running correlations between ZWI/P and ZWI/$\delta^{18}O_{precip}$ in East Africa exhibit multidecadal variations similar to those discussed in section 3.2, with strongest correlations from 1940 to 1970 and weak correlations in the early 20th century (not shown).

We note that the choice of cutoff frequency does not affect these results. The low-frequency SST field correlations are similar at

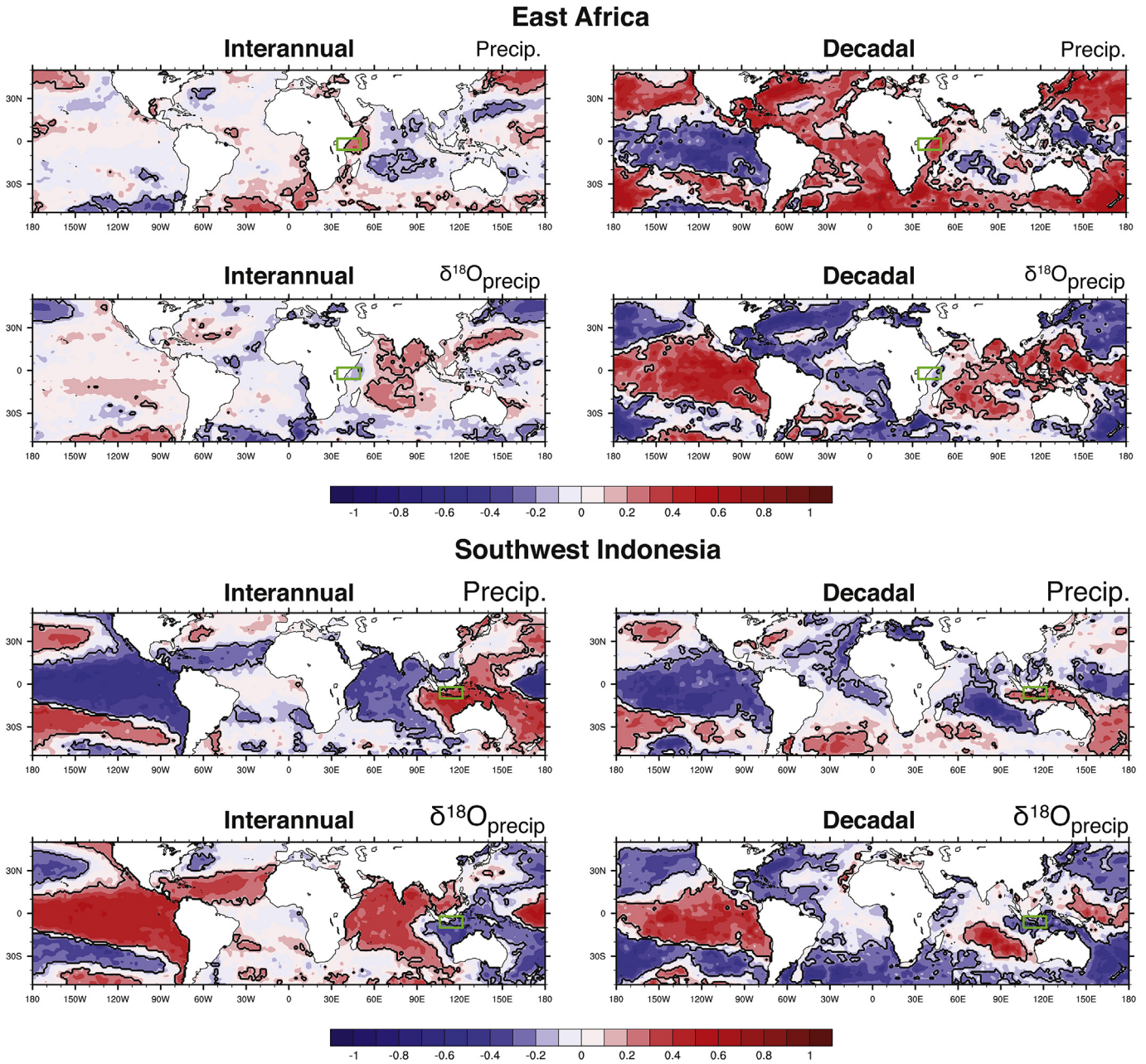


**Fig. 10.** Top: Correlation between East African SST, P and $\delta^{18}O_{precip}$ on interannual (left; high-pass filtered) and decadal (right; low-pass filtered) timescales in the SWING simulation. All data are SOND. Bottom: As in top, but for SW Indonesia.

cutoff frequencies less than ~0.2 (i.e., greater than 5 years). However, these results should be confirmed with a longer simulation in order to robustly test the influence of decadal and multi-decadal SST variations on the IOZM's influence.

## 4. Low-frequency IOZM behavior during the past millennium in precipitation isotopic proxy archives

Our results from the SWING simulation support previous observational and model evidence that the IOZM's spatial influence is broader in East African and SW Indonesian $\delta^{18}O_{precip}$ and $\delta D_{precip}$ than in its imprint on precipitation amount alone (Vuille et al., 2005a). Given this broad regional influence on $\delta^{18}O_{precip}/\delta D_{precip}$ (Section 3.1 and Vuille et al., 2005a), it follows that a collection of spatially distributed proxy archives of $\delta^{18}O_{precip}/\delta D_{precip}$ from both poles of the IOZM may be especially well suited to detect its behavior. Anti-correlated rainfall and $\delta^{18}O_{precip}/\delta D_{precip}$ anomalies in East Africa and Indonesia are not just characteristic of the IOZM, but are likely to occur in response to modifications to the Walker circulation over the Indian Ocean. Our approach is therefore to seek significant but opposing behaviors in $\delta^{18}O_{precip}/\delta D_{precip}$ proxy archives on either side of the Indian Ocean. To this aim, we analyzed six proxy records of $\delta^{18}O_{precip}/\delta D_{precip}$ from continental archives in the IOZM region (Fleitmann et al., 2007; Griffiths et al., 2010; Tierney et al., 2011, 2010; Konecky et al., 2013; Konecky et al., 2014), according to the selection criteria presented in Section 2.2. Information about the proxy records is presented in Table 6.

### 4.1. Links in an IOZM-region proxy data network

The raw time series data that we analyzed are shown in Fig. 11. Using each site's original, published age model, 8 similarity

**Table 6**
Summary of records in IOZM proxy data network.

| Site | Lat | Lon | Proxy | Avg resolution from 850 to 2000 C.E. (years) | Reference |
|---|---|---|---|---|---|
| Dimarshim Cave, Socotra Island, Yemen | 12.3 | 53.4 | Cave $\delta^{18}O$ | 12 | Fleitmann et al. (2007) |
| Sacred Lake, Kenya | 0.05 | 37.5 | Leaf wax δD | 15 | Konecky et al. (2014) |
| Lake Challa, Tanzania | −3.3 | 37.7 | Leaf wax δD | 36 | Tierney et al. (2011) |
| Makassar Strait, Indonesia | −3.9 | 119.4 | Leaf wax δD | 26 | Tierney et al. (2010) |
| Lake Lading, Java, Indonesia | −8 | 113.3 | Leaf wax δD | 8 | Konecky et al. (2013) |
| Liang Luar Cave, Flores, Indonesia | −8.5 | 120.4 | Cave $\delta^{18}O$ | 12 | Griffiths et al. (2009) |

estimates among the six isotope records in the network were found to be significant at the 90% level (Table 7). These similarities are concentrated into five links (Fig. 12, Table 7). Two of these links, between Sacred/Lading (LS = 0.5) and between Challa/Socotra (LS = 0.5), are linearly correlated regardless of which sampling method is used (Gaussian kernels vs. interpolation). The link between Lading/Socotra is just as strong (LS = 0.5) and is significant regardless of which sampling method is used, but the similarities are nonlinear. The other two links (Challa/Makassar and Lading/Makassar) are weaker (LS = 0.25). In these cases, Gaussian kernel sampling yielded significant links whereas linear interpolation did not. The strongest links in the network, where at least two similarity tests yield significant results, are between Sacred/Lading, Challa/Socotra, and Socotra/Lading (Fig. 12a). The link between Sacred/Lading exhibits a negative linear correlation, while the link between Challa/Socotra exhibits a positive linear correlation – consistent with an IOZM-like anti-correlation on either side of the Indian Ocean.

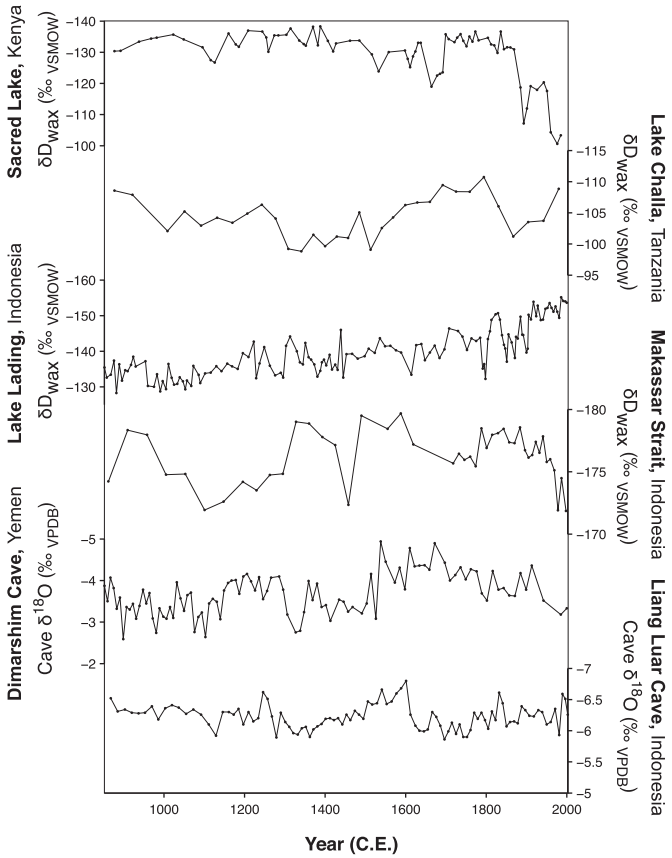


**Fig. 11.** Raw data from all 6 ~1 ka isotopic proxy records from the IOZM region used in our proxy data synthesis.

When age model uncertainties are considered explicitly, only the links between Sacred/Lading and Lading/Socotra remain significant (Fig. 12b). Of the two, the Sacred/Lading link is strongest, and it is strong across all timescales (ensemble mean LS ≥ 0.5). Ensemble mean LS is higher when sub-decadal variability and long-term trends are preserved, rather than on multi-decadal, centennial, and multi-centennial timescales (Fig. 13). The sign of this relationship cannot be assessed through the total link strength, but it can be assessed via linear correlation: The two sites are strongly, negatively correlated when gXCF is considered alone (ensemble mean gXCF LS > 0.9 on all timescales; not shown).

The Lading/Socotra age-uncertain link is more moderate in its strength, and is highly timescale-dependent (Fig. 13). Ensemble mean LS exceeds 0.5 only when the longest-term trends are preserved, and it weakens considerably when these trends are removed. The link is weakest when sub-decadal variability is smoothed, even when the long-term trend is preserved. Hence, long-term trends and high-frequency variability are wholly responsible for the strength of this link. Unlike Sacred/Lading, the two sites are moderately, positively correlated when gXCF is considered alone (ensemble mean gXCF LS > 0.4 at its strongest, when sub-decadal and long-term variability are preserved).

The low sampling resolution and age model uncertainties in the Lake Challa and Makassar Strait records cause links associated with these sites to become null, particularly once detrending and smoothing are introduced.

### 4.2. Implications for IOZM-region proxy reconstructions over the past millennium

We sought to detect IOZM behavior over the past millennium by identifying strong, anti-correlated links in isotopic proxy records from either pole of the IOZM region. Using published age models,

**Table 7**
Summary of significant links in IOZM region isotopic proxy data network (383.3 [*N*/3] yr detrend).

| Record i[a] | Record j[a] | Link strength | Measure[b] | Estimated similarity[c,d] |
|---|---|---|---|---|
| 1. Sacred | **Lading** | 0.5 | gXCF | −0.52 (−0.29, 0.31) |
| | | | iXCF | −0.33 (−0.24, 0.25) |
| 2. Challa | **Socotra** | 0.5 | gXCF | 0.43 (−0.28, 0.30) |
| | | | iXCF | 0.40 (−0.29, 0.30) |
| 3. Lading | **Socotra** | 0.5 | gMI | 0.77 (0.64, 0.76) |
| | | | iMI | 0.99 (0.93, 0.99) |
| 4. Challa | Makassar | 0.25 | gMI | 0.93 (0.83, 0.92) |
| 5. Lading | Makassar | 0.25 | gMI | 0.8626 (0.7171, 0.8388) |

[a] **Bold** = Link is significant using both Gaussian kernel and interpolation techniques.
[b] Only measures that were significant at the 90% level are reported.
[c] Numbers in parentheses represent the upper/lower CI limit from 100 surrogates.
[d] Positive and negative correlations apply to linear cross-correlation functions only. Mutual information tests are directionless (i.e. only positive numbers are possible).

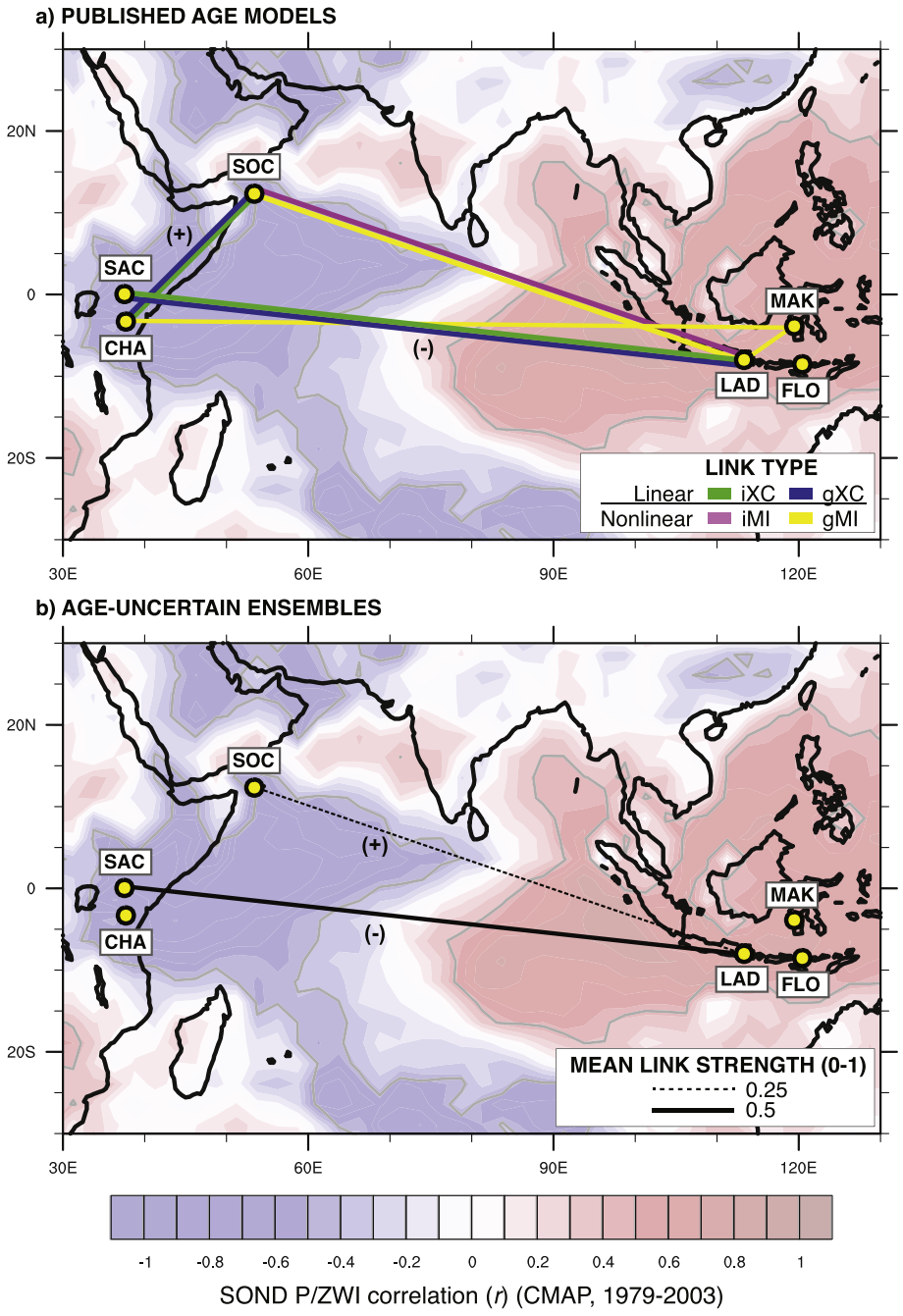


**Fig. 12.** Map showing the locations of the 6 isotopic proxy records used in our synthesis. Yellow circles, site locations of Socotra Island (SOC), Sacred Lake (SAC), Lake Challa (CHA), Lake Lading (LAD), Flores (FLO), and the Makassar Strait (MAK). Shaded regions represent the correlation between ZWI and precipitation amount during the SOND season using NCEP Reanalysis winds and CMAP precipitation, 1979–2003. Bold contours indicate correlation is significant at $p < 0.05$. a) Results of similarity tests using each site's published age model and a ~400 year detrend to remove long-term variability. Significant linear links are shown in blue (iXCF) and green (gXCF) lines, and nonlinear links are shown in pink (iMI) and yellow (gMI) lines. For the linear links, (+) and (−) symbols indicate the sign of the correlation using the gXCF estimator. b) Results of similarity tests using ensembles of 100 perturbed age models for each site (see text). Only links that attained a mean link strength of 0.25 or 0.5 within the multi-centennial timescale are shown. The (+) and (−) symbols indicate the sign of the correlation when only the gXCF is considered.

two of the three strongest links (Sacred/Lading and Lading/Socotra) are between sites on opposite sides of the Indian Ocean, rather than between sites that are adjacent to one another. This indicates that while individual regions exhibit pronounced heterogeneity, cross-Indian-Ocean climate phenomena may be an important driver of climate variability during the past millennium. While it is impossible to distinguish IOZM-like from ENSO-like variability based on this proxy data network alone, the IOZM's observed low-frequency periodicity (Ashok et al., 2004a, 2003) makes it a highly plausible candidate for coherent climate variability during the past millennium.

However, the nonlinear connection between Lading/Socotra indicates that potential IOZM behavior in paleoclimate records is not straightforward. Potential nonlinearities could arise from issues within the proxy records themselves: Lading and Socotra have different seasonal rainfall regimes that could make them

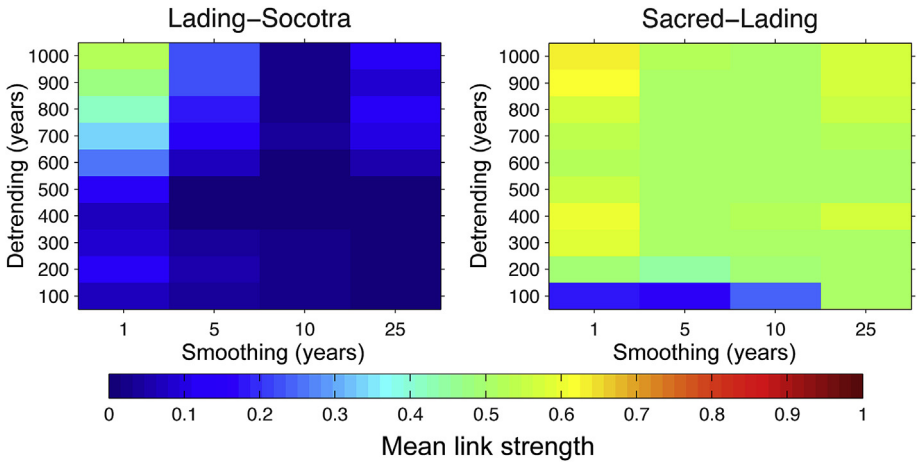


**Fig. 13.** Mean link strengths of age-perturbed ensembles using all similarity estimators (gXCF, iXCF, gMI, iMI) under combinations of smoothing (*x*-axes) and detrending (*y*-axes). In each plot, the quadrants correspond to the following: upper-left, sub-decadal variability with long-term trends preserved; lower-left, sub-decadal variability with long-term trends removed; upper-right, multi-decadal variability with long-term trends preserved; lower-right, multi-decadal variability with long-term trends removed. Centennial and multi-centennial variability are best preserved between 100–300 and 400–600 years, respectively (see text and table of defined timescales). Note that most analyses fail when the detrending window is too small (<100 years).

vulnerable to low-frequency variations in the Indian Monsoon and the ITCZ, but on different timescales (Scholte and De Geest, 2010; Konecky et al., 2013). In addition, the Socotra stalagmite contains no age control points during the past millennium; changes in growth rate are therefore unconstrained, and could lead to non-linearities in the correlations with the IOZM and with other proxy records.

Of the 9 possible significant cross-Indian Ocean links, the Sacred/Lading link is the only connection emerging from our analysis that could be attributed to classic IOZM-like behavior – i.e. periods of more intense/frequent IOZM events affecting the amount of rainfall, and hence $\delta D_{precip}$, during the main IOZM season at both sides of the Indian Ocean Walker cell. The link between Sacred/Lading is the only link in the network to exhibit strong (LS > 0.5), linear, anti-correlated behavior across both sides of the Indian Ocean. This strong negative linear correlation persists across multiple timescales when both the published age models and the age-uncertain ensembles are considered, and is robust even considering age model uncertainties (Table 8, Figs. 12–13). Opposing behavior in $\delta D_{precip}$ in East Africa and SW Indonesia is therefore a robust feature of the isotopic regime during the past millennium, at least at these two sites. The linear relationship suggests that this relationship is relatively straightforward, with D-depleted East African precipitation occurring alongside D-enriched SW Indonesian precipitation, and vice versa. However, a moderate link also exists between Lading/Socotra, and this link is robust considering quantifiable age model uncertainties. Both records have high (~decadal) resolution, and therefore any possible multi-decadal to multi-centennial IOZM variability over the past millennium should be detectable. The nonlinear component of this link and its positive linear correlation indicate that if IOZM variability exists in these two records, it is indirect, or nonstationary.

**Table 8**
Summary of mean link strengths, age-uncertain ensembles.

| Detrend (yr) | 300 | | 600 | | 900 | |
|---|---|---|---|---|---|---|
| Smooth (yr) | 1 | 25 | 1 | 25 | 1 | 25 |
| Lading-Flores | 0.04 | 0.00 | 0.05 | 0.00 | 0.07 | 0.00 |
| Lading-Socotra | 0.09 | 0.00 | 0.25 | 0.05 | 0.47 | 0.09 |
| Sacred-Flores | 0.01 | 0.00 | 0.01 | 0.00 | 0.01 | 0.00 |
| Sacred-Lading | 0.59 | 0.51 | 0.52 | 0.51 | 0.62 | 0.56 |
| Sacred-Socotra | 0.05 | 0.00 | 0.06 | 0.00 | 0.10 | 0.00 |
| Socotra-Flores | 0.10 | 0.03 | 0.12 | 0.03 | 0.16 | 0.01 |

In light of our results from the ECHAM4 SWING simulation (Section 3), nonstationary behavior in the IOZM/$\delta^{18}O_{precip}$ relationship can alter the spatial precipitation/$\delta^{18}O_{precip}$ footprint of the IOZM. This may explain why significant cross-Indian Ocean linkages are so limited over the past millennium: Individual proxy records may fall in and out of the zone of high IOZM/$\delta^{18}O_{precip}$ correlation, leading to inconsistent cross-Indian Ocean connections between sites and lowering their overall similarity. The link between Lading/Socotra could easily be affected by this behavior, as Socotra is located at the edge of the zone of strong IOZM/P correlation in modern observations (Figs. 2 and 5). Because the Sacred/Lading link remains strong on nearly all timescales, a complete disappearance of significant IOZM/$\delta^{18}O_{precip}$ correlation over Indonesia (Fig. 5) could be overestimated in the SWING simulation. Still, we expect that the IOZM's influence diminishes eastward over Indonesia, with sites like Makassar and Flores responding either less strongly or more inconsistently to IOZM variations.

Secondly, at sites with complex controls on $\delta D_{precip}$ – either because of a complex climate or because of an abundance of fractionating processes driving $\delta D_{precip}$ – it may be difficult to detect IOZM behavior on a consistent basis throughout the past millennium. This inconsistency is likely to be even more important on longer paleoclimate timescales when changes in orbital insolation altered the seasonal distribution of rainfall, and hence the relative importance of the seasonally-locked IOZM compared with other climate phenomena.

Finally, our results from the SWING simulation suggest that the positive mode of the IOZM may be more detectable in proxy reconstructions than the negative mode (Section 3.4). This could be an important factor in the limited links among sites in the IOZM region: Periods of time with strong IOZM-positive behavior may last only for several decades or centuries, potentially in response to external forcings, while periods of IOZM-negative behavior may not register in proxies, leading to an inconsistent relationship when one millennium is considered as a whole.

## 5. A data/model perspective on low-frequency IOZM variability

Both our model and our proxy synthesis results indicate the importance of distinguishing whether the IOZM itself varied over the past millennium, or whether its correlation with P and

$\delta^{18}O_{precip}/\delta D_{precip}$ varied. The ECHAM4 SWING experiment shows that when the 134 years are considered as a whole, the ZWI is moderately but significantly ($p < 0.05$) correlated with both P and $\delta^{18}O_{precip}$ in East Africa and SW Indonesia. The IOZM influences $\delta^{18}O_{precip}$ across a broad region, extending beyond its imprint on precipitation amount. This broad spatial footprint in $\delta^{18}O_{precip}$ could theoretically be advantageous to proxy reconstructions of $\delta^{18}O_{precip}$ and $\delta D_{precip}$, as a network of these sites distributed throughout the IOZM-influenced region could potentially be used to reconstruct its behavior through time. Based on these results alone, one could argue that 1) isotopic proxy records from both East Africa and SW Indonesia could be appropriate for reconstructing variations in the IOZM over the past millennium; and 2) both interannual and intrinsic low-frequency variations in the IOZM can be adequately captured by proxy records.

However, the limited number and strength of links in the IOZM proxy data network, even when age model uncertainties are not taken into account, suggest that low-frequency IOZM behavior is difficult to capture in proxy records. Our results from the SWING simulation provide two possible explanations for this lack of coherent variability. First, multi-decadal variations in the strength and spatial signature of the ZWI/P and ZWI/$\delta^{18}O_{precip}$ correlations are evident throughout the SWING simulation. This correlation is especially variable in SW Indonesia where local air-sea interactions and Pacific SSTs can strongly affect precipitation amounts during SOND (Figs. 8–9), but proxy reconstructions from both poles of the IOZM are vulnerable to nonstationarities in the IOZM/$\delta^{18}O_{precip}$ relationship. Second, the positive mode of the IOZM may be more reliably reconstructed using either P or $\delta^{18}O_{precip}$ than its negative mode. Therefore, paleorecords may be most able to capture IOZM+ modes, rather than IOZM- or IOZM-neutral modes. These results add to a growing body of evidence for non-stationary relationships between modes of oceanic/atmospheric circulation and continental precipitation at various timescales during the past millennium (Clark et al., 2003; Zinke et al., 2004; MacDonald and Case, 2005; Stevenson, 2012; Coats et al., 2013).

A confounding factor in any multi-proxy synthesis of $\delta^{18}O$ and $\delta D$ records is the fidelity of each record's reconstructed $\delta^{18}O_{precip}$ to actual $\delta^{18}O_{precip}$. In theory, $\delta^{18}O_{cave}$ and $\delta D_{wax}$ should record the same precipitation isotopic signature, and offsets are often assumed to be relatively constant such that one permil variation in $\delta^{18}O_{cave}$ ($\delta D_{precip}$) translates to one permil variation in $\delta^{18}O_{precip}$ ($\delta D_{wax}$). However, site-specific groundwater regimes, karst hydrology, substrate, cave morphometry, and other factors can alter the transfer function between $\delta^{18}O_{precip}$ and $\delta^{18}O_{cave}$ recorded in speleothems (Baker et al., 2012; Partin et al., 2012; Treble et al., 2013). Similarly, a host of biophysical and ecological factors affect the relationship between $\delta D_{precip}$ and $\delta D_{wax}$, including plant type, leaf structure, root depth, canopy height, and ecosystem type (Sachse et al., 2012 and refs therein), and the residence time of waxes on land affects their representation in the sedimentary record (e.g., Li et al., 2011). These site-level characteristics have been addressed or assumed to be of minor import by the authors of each of the 6 studies used in our IOZM proxy network (Fleitmann et al., 2007; Griffiths et al., 2009; Tierney et al., 2011, 2010; Konecky et al., 2014, 2013). However, these factors could obfuscate potential links between sites in the network. Differences in seasonal rainfall regimes and interannual variability from site to site could also alter potential linkages among sites. These issues are inherent to any synthesis of paleoclimate data from multiple proxies and site locations. Further development of proxy system models for caves and leaf waxes, and "pseudoproxy" experiments (e.g., Cobb et al., 2013) with isotope-equipped paleoclimate simulations, will greatly improve data/model comparison efforts in future studies.

Our proxy data synthesis reveals that, although $\delta^{18}O_{precip}$ and $\delta D_{precip}$ in the region varied considerably from 850 to 2000 C.E., the IOZM is difficult to consistently detect. While this could indicate that processes distinct from the IOZM dominate climate variability in East Africa and Indonesia, results from the SWING simulation imply that this does not necessarily indicate that the IOZM itself was not active over the past millennium. Low-frequency modes of local, tropical and extratropical climate variability can interfere with or enhance the correlation between the IOZM, precipitation, and $\delta^{18}O_{precip}/\delta D_{precip}$, leading proxies to respond with more or less fidelity regardless of the actual strength of IOZM events. Local air-sea interactions and SST variability in the Pacific Ocean appear to exert a particular influence on simulated P and $\delta^{18}O_{precip}$ in SW Indonesia during SOND, the IOZM's active season. The SWING simulation suggests that low-frequency Pacific Ocean SST variability may help to enhance or dampen the degree to which proxies record the IOZM, a finding that should be investigated in future long simulations.

Overall, the complex climatic influences on $\delta^{18}O/\delta D_{precip}$ may complicate the potential IOZM signal in paleoclimate records. That the IOZM/P and IOZM/$\delta^{18}O_{precip}$ relationships are significantly correlated when the 134-year SWING simulation is considered as a whole, but non-stationary on a multi-decadal basis, could indicate that the stationarity of the IOZM signal is timescale-dependent— in other words, centennial or multi-centennial variations in the IOZM can be detected reliably by P and $\delta^{18}O_{precip}$ proxies while multi-decadal variations cannot. The complete lack of strong multi-decadal link strength in our proxy data network, and the reduced strength of the link between Sacred/Lading on multi-centennial timescales, provides further support for this idea. The SWING simulation is not long enough to test the stationarity of the IOZM on centennial and longer timescales, but we anticipate that future isotope-enabled simulations of the past millennium can make significant progress in this arena.

## 6. Conclusions

It is difficult, if not impossible, to assess IOZM-like variability in paleoclimate time series based on individual records, or based on East Africa—or Indonesia-specific groupings. Many climatic processes influence variability in P and $\delta^{18}O_{precip}/\delta D_{precip}$ in each respective region. SOND season precipitation anomalies are highly influential on interannual P and $\delta^{18}O_{precip}/\delta D_{precip}$ in both East Africa and in SW Indonesia. However, tropical $\delta D_{wax}$ and $\delta^{18}O_{cave}$ proxies by nature integrate a year-round signal, and could be influenced by climatic phenomena other than the IOZM, including variations in the Indian, African, and Australasian monsoons. A distinctive spatial imprint of low-frequency Indian Ocean variability that could be deemed IOZM-like may be evident in East African precipitation (Tierney et al., 2013), but our model results (Section 3) show that the IOZM's spatial footprint likely migrates, waxes, and wanes through time. SW Indonesia appears particularly susceptible to multi-decadal variations in the correlation between ZWI, P, and $\delta^{18}O_{precip}$, while correlations in East Africa are more stable. Given this finding, attempts to reconstruct the IOZM on paleoclimate timescales using Indonesian proxy records (cf. Section 4) could face difficulties, as changes in the strength of the ZWI correlations in SW Indonesia would influence the strength of cross-Indian Ocean linkages.

We conclude that on multi-decadal (and possibly longer) timescales, the IOZM+ mode may be able to explain certain paleoclimate variations in the Indian Ocean region, particularly when reconstructed through $^{18}O$- and D-isotopic archives. However, IOZM− modes serve as less robust analogies, and IOZM variations should generally be used with caution when interpreting paleoclimate records unless there is strong evidence for an IOZM-

positive mode in Indian Ocean SSTs – a question that is currently difficult to assess with the limited number of SST records from the Western Equatorial Indian Ocean. From the SWING simulation, we note that the nature of low-frequency variations in the IOZM is likely due to periods of more intense or frequent interannual events, rather than intrinsic modes of variability in the Indian Ocean. Low-frequency modes of variability in extratropical Pacific Ocean SST may play a role in modulating the relationship between the IOZM and $P/\delta^{18}O_{precip}$ in the region, particularly in SW Indonesia, where the effects are most obvious. Overall, whether the strength of the IOZM itself varied over the past millennium, or whether the strength of the IOZM's correlation with P and $\delta^{18}O_{precip}/\delta D_{precip}$ varied, remains to be seen in longer, fully-coupled, isotope-enabled model experiments and in additional isotopic proxy records.

## Acknowledgments

This project was supported by NOAA grant NOAA-NA090AR4310107 to J. Russell, NOAA grant NA09OAR4310090 and NSF AGS grant 1003690 to M. Vuille, and by an NSF Graduate Research Fellowship to B. Konecky. We thank three anonymous reviewers for helpful feedback on this manuscript.

## Appendix A. Supplementary data

Supplementary data related to this article can be found at http://dx.doi.org/10.1016/j.quascirev.2014.08.019.

## References

Abram, N.J., Gagan, M.K., Cole, J.E., Hantoro, W.S., Mudelsee, M., 2008. Recent intensification of tropical climate variability in the Indian Ocean. Nat. Geosci. 1, 849–853.
Abram, N.J., Gagan, M.K., Liu, Z., Hantoro, W.S., McCulloch, M.T., Suwargadi, B.W., 2007. Seasonal characteristics of the Indian Ocean Dipole during the Holocene epoch. Nature 445, 299–302.
Aldrian, E., Susanto, R., 2003. Identification of three dominant rainfall regions within Indonesia and their relationship to sea surface temperature. Int. J. Climatol. 23, 1435–1452.
Anchukaitis, K.J., Tierney, J.E., 2012. Identifying coherent spatiotemporal modes in time-uncertain proxy paleoclimate records. Clim. Dyn. http://dx.doi.org/10.1007/s00382-012-1483-0.
Annamalai, H., Murtugudde, R., Potemra, J., Xie, S., Liu, P., Wang, B., 2003. Coupled dynamics over the Indian Ocean: spring initiation of the Zonal Mode. Deep-Sea Res. Pt II 50, 2305–2330.
Annamalai, H., Potemra, J., Murtugudde, R., McCreary, J.P., 2005. Effect of preconditioning on the extreme climate events in the tropical Indian Ocean. J. Clim. 18, 3450–3469.
Ashok, K., Chan, W.L., Motoi, T., Yamagata, T., 2004a. Decadal variability of the Indian Ocean Dipole. Geophys. Res. Lett. 31 (L24), 207.
Ashok, K., Guan, Z., Saji, N.H., Yamagata, T., 2004b. Individual and combined influences of ENSO and the Indian Ocean Dipole on the Indian summer monsoon. J. Clim. 17, 3141–3155.
Ashok, K., Guan, Z., Yamagata, T., 2001. Impact of the Indian Ocean Dipole on the relationship between the Indian monsoon rainfall and ENSO. Geophys. Res. Lett. 28, 4499–4502.
Ashok, K., Guan, Z., Yamagata, T., 2003. A look at the relationship between the ENSO and the Indian Ocean Dipole. J. Meteorol. Soc. Jpn. 81, 41–56.
Baker, A., Bradley, C., Phipps, S.J., Fischer, M., Fairchild, I.J., Fuller, L., Spötl, C., Azcurra, C., 2012. Millennial-length forward models and pseudoproxies of stalagmite $\delta^{18}O$: an example from NW Scotland. Clim. Past Discuss. 8, 869–907.
Behera, S.K., Luo, J.-J., Masson, S., Rao, S.A., Sakuma, H., Yamagata, T., 2006. A CGCM study on the interaction between IOD and ENSO. J. Clim. 19, 1688–1705.
Blaauw, M., Christen, J.A., 2011. Flexible paleoclimate age-depth models using an autoregressive gamma process. Bayesian Anal. 6, 457–474.
Black, E., Slingo, J., Sperber, K.R., 2003. An observational study of the relationship between excessively strong short rains in coastal East Africa and Indian Ocean SST. Mon. Weather Rev. 131, 74–94.
Cai, W., Sullivan, A., Cowan, T., 2009. Climate change contributes to more frequent consecutive positive Indian Ocean Dipole events. Geophys. Res. Lett. 36 (L23), 704.
Cai, W., Zheng, X.-T., Weller, E., Collins, M., Cowan, T., Lengaigne, M., Yu, W., Yamagata, T., 2013. Projected response of the Indian Ocean Dipole to greenhouse warming. Nat. Geosci. 6, 999–1007.
Clark, C.O., Webster, P.J., Cole, J.E., 2003. Interdecadal variability of the relationship between the Indian Ocean Zonal Mode and East African coastal rainfall anomalies. J. Clim. 16, 548–554.
Coats, S., Smerdon, J.E., Cook, B.I., Seager, R., 2013. Stationarity of the tropical Pacific teleconnection to North America in CMIP5/PMIP3 model simulations. Geophys. Res. Lett. 40, 4927–4932.
Cobb, K., Charles, C., Cheng, H., 2003. El Nino/Southern oscillation and tropical Pacific climate during the last millennium. Nature 424, 271–276.
Cobb, K.M., Westphal, N., Sayani, H.R., Watson, J.T., Di Lorenzo, E., Cheng, H., Edwards, R.L., Charles, C.D., 2013. Highly variable El Nino-southern oscillation throughout the Holocene. Science 339, 67–70.
Compo, G.P., Whitaker, J.S., Sardeshmukh, P.D., Matsui, N., Allan, R.J., Yin, X., Gleason, B.E., Vose, R.S., Rutledge, G., Bessemoulin, P., Brönnimann, S., Brunet, M., Crouthamel, R.I., Grant, A.N., Groisman, P.Y., Jones, P.D., Kruk, M., Kruger, A.C., Marshall, G.J., Maugeri, M., Mok, H.Y., Nordli, Ø., Ross, T.F., Trigo, R.M., Wang, X.L., Woodruff, S.D., Worley, S.J., 2011. The twentieth century reanalysis project. Q. J. R. Meteorol. Soc. 137, 1–28. http://dx.doi.org/10.1002/qj.776.
Conroy, J.L., Cobb, K.M., Noone, D., 2013. Comparison of precipitation isotope variability across the tropical Pacific in observations and SWING2 model simulations. J. Geophys. Res-Atmos. 118, 5867–5892.
Conroy, J.L., Overpeck, J.T., Cole, J.E., Shanahan, T.M., Steinitz-Kannan, M., 2008. Holocene changes in eastern tropical Pacific climate inferred from a Galápagos lake sediment record. Quat. Sci. Rev. 27, 1166–1180.
Costa, K., Russell, J., Konecky, B., Lamb, H., 2014. Isotopic reconstruction of the African Humid period and Congo air boundary migration at Lake Tana, Ethiopia. Quat. Sci. Rev. 83, 58–67.
D'Arrigo, R., Allan, R., Wilson, R., Palmer, J., Sakulich, J., Smerdon, J.E., Bijaksana, S., Ngkoimani, L.O., 2008. Pacific and Indian Ocean climate signals in a tree-ring record of Java monsoon drought. Int. J. Climatol. 28, 1889–1901.
D'Arrigo, R., Smerdon, J.E., 2008. Tropical climate influences on drought variability over Java, Indonesia. Geophys. Res. Lett. 35, L05707.
Dansgaard, W., 1964. Stable isotopes in precipitation. Tellus 16, 436–468.
Donges, J.F., Zou, Y., Marwan, N., Kurths, J., 2009. The backbone of the climate network. Europhys. Lett. 87, 48007.
Enfield, D.B., Mestas-Nuñez, A.M., 1999. Multiscale variabilities in global sea surface temperatures and their relationships with tropospheric climate patterns. J. Clim. 12, 2719–2733.
Felis, T., Merkel, U., Asami, R., Deschamps, P., Hathorne, E.C., Kölling, M., Bard, E., Cabioch, G., Durand, N., Prange, M., Schulz, M., Cahyarini, S.Y., Pfeiffer, M., 2012. Pronounced interannual variability in tropical South Pacific temperatures during Heinrich Stadial 1. Nat. Commun. 3, 965. http://dx.doi.org/10.1038/ncomms1973.
Fischer, A.S., Terray, P., Guilyardi, E., Gualdi, S., Delecluse, P., 2005. Two independent triggers for the Indian Ocean Dipole/Zonal Mode in a coupled GCM. J. Clim. 18, 3428–3449.
Fleitmann, D., Burns, S.J., Mangini, A., Mudelsee, M., Kramers, J., Villa, I., Neff, U., Al-Subbary, A.A., Buettner, A., Hippler, D., 2007. Holocene ITCZ and Indian monsoon dynamics recorded in stalagmites from Oman and Yemen (Socotra). Quat. Sci. Rev. 26, 170–188.
Gnanaseelan, C., Vaid, B.H., 2010. Interannual variability in the Biannual Rossby waves in the tropical Indian Ocean and its relation to Indian Ocean Dipole and El Nino forcing. Ocean Dyn. 60, 27–40.
Griffiths, M.L., Drysdale, R.N., Gagan, M.K., Frisia, S., Zhao, J.-X., Ayliffe, L.K., Hantoro, W.S., Hellstrom, J.C., Fischer, M.J., Feng, Y.-X., Suwargadi, B.W., 2010. Evidence for Holocene changes in Australian-Indonesian monsoon rainfall from stalagmite trace element and stable isotope ratios. Earth Planet. Sci. Lett. 292, 27–38.
Griffiths, M.L., Drysdale, R.N., Gagan, M.K., Zhao, J.X., Ayliffe, L.K., Hellstrom, J.C., Hantoro, W.S., Frisia, S., Feng, Y.X., Cartwright, I., Pierre, E.S., Fischer, M.J., Suwargadi, B.W., 2009. Increasing Australian-Indonesian monsoon rainfall linked to early Holocene sea-level rise. Nat. Geosci. 2, 636–639.
Gupta, A.K., Sarkar, S., De, S., Clemens, S.C., Velu, A., 2010. Mid-Brunhes strengthening of the Indian Ocean Dipole caused increased equatorial East African and decreased Australasian rainfall. Geophys. Res. Lett. 37 (L06), 706.
Hastenrath, S., 2005. Mechanisms of climate anomalies in the equatorial Indian Ocean. J. Geophys. Res. 110 (D08), 113.
Hastenrath, S., Nicklis, A., Greischar, L., 1993. Atmospheric-hydrospheric mechanisms of climate anomalies in the western equatorial Indian Ocean. J. Geophys. Res. 98, 219–235.
Hendon, H.H., 2003. Indonesian rainfall Variability: impacts of ENSO and local Air–Sea interaction. J. Clim. 16, 1775–1790.
IAEA/WMO, 2006. Global Network of Isotopes in Precipitation. The GNIP Database. Accessible at: http://www.iaea.org/water.
Ihara, C., Kushnir, Y., Cane, M.A., 2008. Warming trend of the Indian Ocean SST and Indian Ocean Dipole from 1880 to 2004. J. Clim. 21, 2035–2046.
Kalnay, et al., 1996. The NCEP/NCAR 40-year reanalysis project. Bull. Am. Meteor. Soc. 77, 437–470.
Klein, S.A., Soden, B.J., Lau, N.-C., 1999. Remote sea surface temperature variations during ENSO: evidence for a tropical atmospheric bridge. J. Clim. 12, 917–932. http://dx.doi.org/10.1175/1520-0442(1999).
Konecky, B., Russell, J., Huang, Y., Vuille, M., Cohen, L., Street-Perrott, F.A., 2014. Impact of monsoons, temperature, and CO2 on the rainfall and ecosystems of Mt. Kenya during the Common Era. Palaeogeogr. Palaeoclimatol. Palaeoecol. 396, 17–25.

Konecky, B.L., Russell, J.M., Rodysill, J.R., Vuille, M., 2013. Intensification of southwestern Indonesian rainfall over the past millennium. Geophys. Res. Lett. 40, 1–6.
Kripalani, R.H., Kumar, P., 2004. Northeast monsoon rainfall variability over south peninsular India vis-à-vis the Indian Ocean Dipole mode. Int. J. Climatol. 24, 1267–1282.
Krishnan, R., Sugi, M., 2003. Pacific decadal oscillation and variability of the Indian summer monsoon rainfall. Clim. Dyn. 21, 233–242.
Levin, N.E., Zipser, E.J., Cerling, T.E., 2009. Isotopic composition of waters from Ethiopia and Kenya: insights into moisture sources for eastern Africa. J. Geophys. Res. 114 (D23), 306.
Li, C., Sessions, A.L., Valentine, D.L., Thiagarajan, N., 2011. D/H variation in terrestrial lipids from Santa Barbara Basin over the past 1400years: a preliminary assessment of paleoclimatic relevance. Org. Geochem. 42, 15–24.
Li, T., Wang, B., Chang, C.-P., Zhang, Y., 2003. A theory for the Indian Ocean Dipole-Zonal Mode. J. Atmos. Sci. 60, 2119–2135.
MacDonald, G.M., Case, R.A., 2005. Variations in the Pacific Decadal oscillation over the past millennium. Geophys. Res. Lett. 32 (L08), 703.
Malik, N., Bookhagen, B., Marwan, N., Kurths, J., 2011. Analysis of spatial and temporal extreme monsoonal rainfall over South Asia using complex networks. Clim. Dyn. 39, 971–987.
Mantua, N.J., Hare, S.R., 2002. The Pacific decadal oscillation. J. Oceanogr. 58, 35–44.
Masson-Delmotte, V., Schulz, M., Abe-Ouchi, A., Beer, J., Ganopolski, A., González-Rouco, J.F., Jansen, E., Lambeck, K., Luterbacher, J., Naish, T., Osborn, T., Otto-Bliesner, B., Quinn, T.M., Ramesh, R., Rojas, M., Shao, X., Timmermann, A., 2013. Information from paleoclimate archives. In: Stocker, T.F., Qin, D., Plattner, G.K., Tignor, M., Allen, S.K., Boschung, J., Nauels, A., Xia, Y., Bex, V., Midgley, P.M. (Eds.), Climate Change 2013: the Physical Science Basis. Contribution of Working Group I to the Fifth Assessment Report of the Intergovernmental Panel on Climate Change. Cambridge University Press, Cambridge, United Kingdom and New York, New York.
Mitchell Jr., J.M., Dzerdzeevskii, B., Flohn, H., Hofmyer, W.L., Lamb, H.H., Kao, K.N., Wallen, C.C., 1966. Climatic Change Technical Note 79. World Meteorological Organization.
Moerman, J.W., Cobb, K.M., Adkins, J.F., Sodemann, H., Clark, B., Tuen, A.A., 2013. Diurnal to interannual rainfall $\delta^{18}O$ variations in northern Borneo driven by regional hydrology. Earth Planet. Sci. Lett. 369-370, 108–119.
Moy, C.M., Seltzer, G.O., Rodbell, D.T., Anderson, D.M., 2002. Variability of El Nino/Southern Oscillation activity at millennial timescales during the Holocene epoch. Nature 420, 162–165.
Newton, A., Thunell, R., Stott, L., 2006. Climate and hydrographic variability in the Indo-Pacific Warm Pool during the last millennium. Geophys. Res. Lett. 33 (L19), 710.
Nicholson, S., 1997. An analysis of the ENSO signal in the tropical Atlantic and western Indian Oceans. Int. J. Climatol. 17, 345–375.
Nicholson, S., Kim, J., 1997. The relationship of the El Niño-southern oscillation to African rainfall. Int. J. Climatol. 17, 117–135.
Nicholson, S.E., 1996. A review of climate dynamics and climate variability in eastern Africa. In: Johnson, T.C., Odada, E.O. (Eds.), The Limnology, Climatology, and Paleoclimatology of the East African Lakes. Gordon and Breach, Amsterdam, The Netherlands, pp. 25–56.
Partin, J.W., Cobb, K.M., Adkins, J.F., Clark, B., Fernandez, D.P., 2007. Millennial-scale trends in west Pacific warm pool hydrology since the Last Glacial Maximum. Nature 449, 452–455.
Partin, J.W., Jenson, J.W., Banner, J.L., Quinn, T.M., Taylor, F.W., Sinclair, D., Hardt, B., Lander, M.A., Bell, T., Miklavič, B., Jocson, J.M.U., Taboroši, D., 2012. Relationship between modern rainfall variability, cave dripwater, and stalagmite geochemistry in Guam, USA. Geochem. Geophys. Geosyst. 13 (Q03), 013.
Rehfeld, K., Kurths, J., 2014. Similarity estimators for irregular and age-uncertain time series. Clim. Past 10 (1), 107–122.
Rehfeld, K., Marwan, N., Breitenbach, S.F., Kurths, J., 2012. Late Holocene Asian summer monsoon dynamics from small but complex networks of paleoclimate data. Clim. Dyn. http://dx.doi.org/10.1007/s00382-012-1448-3.
Rehfeld, K., Marwan, N., Heitzig, J., Kurths, J., 2011. Comparison of correlation analysis techniques for irregularly sampled time series. Nonlinear Process. Geophys. 18, 389–404.
Rodysill, J.R., Russell, J.M., Bijaksana, S., Brown, E.T., Safiuddin, L.O., Eggermont, H., 2012. A paleolimnological record of rainfall and drought from East Java, Indonesia during the last 1,400 years. J. Paleolimnol. 47, 125–139.
Rodysill, J.R., Russell, J.M., Crausbay, S.D., Bijaksana, S., Vuille, M., Edwards, R.L., Cheng, H., 2013. A severe drought during the last millennium in East Java, Indonesia. Quat. Sci. Rev. 80, 102–111.
Sachse, D., Billault, I., Bowen, G.J., Chikaraishi, Y., Dawson, T.E., Feakins, S.J., Freeman, K.H., Magill, C.R., McInerney, F.A., van der Meer, M.T.J., 2012. Molecular paleohydrology: Interpreting the hydrogen-isotopic composition of lipid biomarkers from photosynthesizing organisms. Annu. Rev. Earth Planet. Sci. 40, 221–249.
Saji, N., Goswami, B., Vinayachandran, P., Yamagata, T., 1999. A dipole mode in the tropical Indian Ocean. Nature 401, 360–363.
Saji, N., Yamagata, T., 2003a. Structure of SST and surface wind variability during Indian ocean Dipole mode events: COADS observations. J. Clim. 16, 2735–2751.
Saji, N., Yamagata, T., 2003b. Possible impacts of Indian Ocean Dipole mode events on global climate. Clim. Res. 25, 151–169.
Saji, N.H., Xie, S.P., Yamagata, T., 2006. Tropical Indian Ocean variability in the IPCC Twentieth-Century climate simulations. J. Clim. 19, 4397–4417.
Scholte, P., De Geest, P., 2010. The climate of Socotra Island (Yemen): a first-time assessment of the timing of the monsoon wind reversal and its influence on precipitation and vegetation patterns. J. Arid Environ. 74, 1507–1515.
Schott, F.A., McCreary Jr., J.P., 2001. The monsoon circulation of the Indian Ocean. Prog. Oceanogr. 51, 1–123.
Schott, F.A., Xie, S.-P., Mccreary, J.P., 2009. Indian Ocean circulation and climate variability. Rev. Geophys. 47.
Sinha, A., Cannariato, K.G., Stott, L.D., Cheng, H., Edwards, R.L., Yadava, M.G., Ramesh, R., Singh, I.B., 2007. A 900-year (600 to 1500 A. D.) record of the Indian summer monsoon precipitation from the core monsoon zone of India. Geophys. Res. Lett. 34 (L16), 707.
Stager, J., Ryves, D., Cumming, B., Meeker, L., Beer, J., 2005. Solar variability and the levels of Lake Victoria, East Africa, during the last millenium. J. Paleolimnol. 33, 243–251.
Stevenson, S.L., 2012. Significant changes to ENSO strength and impacts in the twenty-first century: results from CMIP5. Geophys. Res. Lett. 39 (L17), 703.
Tierney, J., Oppo, D., Rosenthal, Y., Russell, J.M., Linsley, B.K., 2010. Coordinated hydrological regimes in the Indo-Pacific region during the past two millennia. Paleoceanography 25 (PA1), 102.
Tierney, J., Russell, J., Sinninghe Damsté, J.S., Huang, Y., Verschuren, D., 2011. Late Quaternary behavior of the East African monsoon and the importance of the Congo Air Boundary. Quat. Sci. Rev. 30, 798–807.
Tierney, J.E., Smerdon, J.E., Anchukaitis, K.J., Seager, R., 2013. Multidecadal variability in East African hydroclimate controlled by the Indian Ocean. Nature 493, 389–392.
Timm, O., Pfeiffer, M., Dullo, W.C., 2005. Nonstationary ENSO-precipitation teleconnection over the equatorial Indian Ocean documented in a coral from the Chagos Archipelago. Geophys. Res. Lett. 32 (L02), 701.
Tozuka, T., Luo, J.-J., Masson, S., Yamagata, T., 2007. Decadal modulations of the Indian Ocean Dipole in the SINTEX-F1 coupled GCM. J. Clim. 20, 2881–2894.
Treble, P.C., Bradley, C., Wood, A., Baker, A., Jex, C.N., Fairchild, I.J., Gagan, M.K., Cowley, J., Azcurra, C., 2013. An isotopic and modelling study of flow paths and storage in Quaternary calcarenite, SW Australia: implications for speleothem paleoclimate records. Quat. Sci. Rev. 64, 90–103.
Ummenhofer, C.C., Gupta, Sen, A., Li, Y., Taschetto, A.S., England, M.H., 2011. Multidecadal modulation of the El Niño–Indian monsoon relationship by Indian Ocean variability. Environ. Res. Lett. 6, 034006.
Vuille, M., Burns, S.J., Taylor, B.L., Cruz, F.W., Bird, B.W., Abbott, M.B., Kanner, L.C., Cheng, H., Novello, V.F., 2012. A review of the South American Monsoon history as recorded in stable isotopic proxies over the past two millennia. Clim. Past Discuss. 8, 637–668.
Vuille, M., Werner, M., Bradley, R.S., Chan, R.Y., Keimig, F., 2005a. Stable isotopes in East African precipitation record Indian Ocean Zonal Mode. Geophys. Res. Lett. 32 (L21), 705.
Vuille, M., Werner, M., Bradley, R.S., Keimig, F., 2005b. Stable isotopes in precipitation in the Asian monsoon region. J. Geophys. Res. 110 (D23), 108.
Webster, P.J., Moore, A.M., Loschnigg, J.P., Leben, R.R., 1999. Coupled ocean-atmosphere dynamics in the Indian Ocean during 1997–98. Nature 401, 356–360.
Xie, P., Arkin, P.A., 1997. Global precipitation: a 17-year monthly analysis based on gauge observations, satellite estimates, and numerical model outputs. Bull. Am. Meteor. Soc. 78, 2539–2558.
Yan, H., Sun, L., Oppo, D.W., Wang, Y., Liu, Z., Xie, Z., Liu, X., Cheng, W., 2011. South China Sea hydrological changes and Pacific Walker circulation variations over the last millennium. Nat. Commun. 2, 293–295.
Zhang, Y., Wallace, J.M., Battisti, D.S., 1997. ENSO-like interdecadal variability: 1900–93. J. Clim. 10, 1004–1020.
Zhao, Y., Braconnot, P., Marti, O., Harrison, S.P., Hewitt, C., Kitoh, A., Liu, Z., Mikolajewicz, U., Otto-Bliesner, B., Weber, S.L., 2005. A multi-model analysis of the role of the ocean on the African and Indian monsoon during the mid-Holocene. Clim. Dyn. 25, 777–800.
Zinke, J., Dullo, W.-C., Heiss, G.A., Eisenhauer, A., 2004. ENSO and Indian Ocean subtropical dipole variability is recorded in a coral record off southwest Madagascar for the period 1659 to 1995. Earth Planet. Sci. Lett. 228, 177–194.
Zinke, J., Pfeiffer, M., Timm, O., Dullo, W.C., Brummer, G., 2009. Western Indian Ocean marine and terrestrial records of climate variability: a review and new concepts on land–ocean interactions since AD 1660. Int. J. Earth Sci. 98, 115–133.